SOCIETY FOR EXPERIMENTAL BIOLOGY

Journal of Experimental Botany, Vol. 74, No. 18 pp. 5854–5869, 2023
https://doi.org/10.1093/jxb/erad285 Advance Access Publication 20 July 2023

RESEARCH PAPER

A dominant-negative avirulence effector of the barley powdery mildew fungus provides mechanistic insight into barley MLA immune receptor activation

Emma E. Crean[1,†], Merle Bilstein-Schloemer[1,†], Takaki Maekawa[1,2,3], Paul Schulze-Lefert[2,3] and Isabel M. L. Saur[1,3,*]

[1] Institute for Plant Sciences, University of Cologne, D-50674 Cologne, Germany
[2] Department for Plant Microbe Interactions, Max-Planck Institute for Plant Breeding Research, D-50829 Cologne, Germany
[3] Cluster of Excellence on Plant Sciences (CEPLAS), Germany

[†] These authors contributed equally to this work.
[*] Correspondence: isabel.saur@uni-koeln.de

Received 16 January 2023; Editorial decision 17 July 2023; Accepted 18 July 2023

Editor: Wen-Ming Wang, Sichuan Agricultural University, China

Abstract

Nucleotide-binding leucine-rich repeat receptors (NLRs) recognize pathogen effectors to mediate plant disease resistance often involving host cell death. Effectors escape NLR recognition through polymorphisms, allowing the pathogen to proliferate on previously resistant host plants. The powdery mildew effector AVR_{A13}-1 is recognized by the barley NLR MLA13 and activates host cell death. We demonstrate here that a virulent form of AVR_{A13}, called AVR_{A13}-V2, escapes MLA13 recognition by substituting a serine for a leucine residue at the C-terminus. Counterintuitively, this substitution in AVR_{A13}-V2 resulted in an enhanced MLA13 association and prevented the detection of AVR_{A13}-1 by MLA13. Therefore, AVR_{A13}-V2 is a dominant-negative form of AVR_{A13} and has probably contributed to the breakdown of *Mla13* resistance. Despite this dominant-negative activity, AVR_{A13}-V2 failed to suppress host cell death mediated by the MLA13 autoactive MHD variant. Neither AVR_{A13}-1 nor AVR_{A13}-V2 interacted with the MLA13 autoactive variant, implying that the binding moiety in MLA13 that mediates association with AVR_{A13}-1 is altered after receptor activation. We also show that mutations in the MLA13 coiled-coil domain, which were thought to impair Ca^{2+} channel activity and NLR function, instead resulted in MLA13 autoactive cell death. Our results constitute an important step to define intermediate receptor conformations during NLR activation.

Keywords: AVR, barley, *Blumeria graminis*, cell death, fungal effector, Mildew Locus A, MLA, NLR, powdery mildew, resistance.

Introduction

During infection of their host, pathogens secrete numerous virulence factors that act extracellularly or inside host cells. These so-called effectors manipulate the host's physiology in favour of the pathogen. Disease resistance of a plant against a pathogen is often mediated by nucleotide-binding leucine-rich repeat receptors (NLRs) (Maekawa *et al.*, 2011b; Jones

Abbreviations: AVR, avirulence effector; *Bgh*, *Blumeria graminia* f.sp. *hordei*; CNL, coiled-coil-type NLR; LRR, leucine-rich repeat; MLA, Mildew Locus A NLR; NB, nucleotide-binding; NLR, nucleotide-binding leucine-rich repeat receptor; RNL, resistance to powdery mildew 8-like NLR; TNL, Toll/interleukin-like-type NLR.

et al., 2016). NLRs recognize effectors directly or by indirectly detecting effector-mediated alterations of host targets (Cesari, 2018). Effector-mediated NLR activation is often linked to localized host cell death (Dodds and Rathjen, 2010; Saur and Hückelhoven, 2021; Maekawa *et al.*, 2022), and recognized effectors are called avirulence (AVR) effectors. Diversification of *AVR* genes can lead to loss of recognition by the respective NLR, resulting in pathogen virulence and breakdown of disease resistance (Märkle *et al.*, 2022). In the case of direct AVR recognition, the NLR can usually no longer bind the diversified effector proteins (Saur *et al.*, 2021).

NLRs are multidomain proteins with a central nucleotide-binding (NB) domain and C-terminal leucine-rich repeats (LRRs). At the N-terminus, most NLRs encode either a Toll/interleukin-1 receptor-like (TIR) or a coiled-coil (CC) domain, classifying the majority of NLRs into either TIR-type NLRs (TNLs) or CC-type NLRs (CNLs) (Shao *et al.*, 2016). A subgroup of CNLs (also called RPW8-like NLRs or RNLs) are the helper NLRs NRG1 (N REQUIREMENT GENE 1) and ADR1 (ACTIVATED DISEASE RESISTANCE GENE 1) that are required for TNL-mediated disease resistance (Saile *et al.*, 2020). The N-terminal CC and TIR domains mediate NLR signal emission upon NLR activation (Swiderski *et al.*, 2009; Bernoux *et al.*, 2011; Collier *et al.*, 2011; Maekawa *et al.*, 2011a; Williams *et al.*, 2014). In inactive receptors, CC and TIR domains are locked in inactive conformations, and this autoinhibition is mediated by interdomain interactions between the N-terminal domains and the NB and LRR domains (Burdett *et al.*, 2019; Saur *et al.*, 2021; Tamborski *et al.*, 2023). Although structural information on intermediate forms between inactive and active NLRs is limited to the structure of the *Arabidopsis thaliana* CNL ZAR1 (HOPZ-ACTIVATED RESISTANCE 1) (Wang *et al.*, 2019b), NLR activation appears to be a multistep process (Förderer *et al.*, 2022b). The first activation step is ligand binding, which induces a steric clash between the LRR and the NB domains. The resulting open conformation of the NB domain then allows ADP (inactive) to ATP (active) exchange, which in turn induces allosteric changes to release the conformational autoinhibition of the CC or TIR domains. This induces NLR oligomerization, and these NLR oligomers are referred to as resistosomes (Förderer *et al.*, 2022b). Certain amino acid replacements within the conserved MHD motif of the NB domain mimic ATP binding and thus result in an active NLR conformation (Dinesh-Kumar and Baker, 2000; Bendahmane *et al.*, 2002; Gao *et al.*, 2011; Bai *et al.*, 2012; Ntoukakis *et al.*, 2013; Roberts *et al.*, 2013; Nishimura *et al.*, 2017). The N-terminal portion of the LRR domain in CNLs also contributes to receptor autoregulation through interactions with CC and NB domains, and amino acid exchanges at these sites can affect NLR autoactivity (Rairdan and Moffett, 2006; Slootweg *et al.*, 2013; Burdett *et al.*, 2019; Förderer *et al.*, 2022a; Tamborski *et al.*, 2023). For receptor activation via direct effector recognition, amino acids in the LRR can also function as effector contact sites and can define the specificity of effector recognition (Jia *et al.*, 2000; Shen *et al.*, 2003; Dodds *et al.*, 2006; Bauer *et al.*, 2021). Upon direct effector recognition by the LRR or other integrated domains, effector binding correlates directly with NLR signal activation, and studies on the *Magnaporthe oryzae* effectors AvrPik and AVR-Pia and the rice NLRs Pik and RGA5 (RESISTANCE GENE ANALOG5), respectively, argue for an affinity threshold between receptor and effector for activation of NLR immune signalling and pathogen resistance (Ortiz *et al.*, 2017; de la Concepcion *et al.*, 2018).

While the mechanisms underlying the restriction of pathogen growth by resistosomes is not fully elucidated, recent cryo-EM structures of multiple resistosomes (Wang *et al.*, 2019a, b; Ma *et al.*, 2020; Martin *et al.*, 2020; Förderer *et al.*, 2022a) revealed fundamental differences in TNL and CNL signalling: the pentameric resistosomes of *A. thaliana* ZAR1 CNL and wheat Sr35 CNL have Ca^{2+} channel activity (Bi *et al.*, 2021; Förderer *et al.*, 2022a). The funnel-shaped ZAR1 cation channel is formed by the N-terminal CC domain α1-helix of the ZAR1 resistosome (Wang *et al.*, 2019a, b). Substitutions of negatively charged amino acids to alanine in the inner lining of the funnel abolish Ca^{2+} channel and cell death activity and ZAR1-mediated resistance (Wang *et al.*, 2019b; Bi *et al.*, 2021). The α1-helix of the wheat Sr35 resistosome is not well resolved and Sr35 α1-helix amino acid exchanges equivalent to those in ZAR1 do not affect Sr35 resistosome channel and cell death activity (Förderer *et al.*, 2022a; Zhao *et al.*, 2022), suggesting differences in Ca^{2+} signalling functions between ZAR1 and Sr35. Effector binding to the TNLs RPP1 (RECOGNITION OF PERONOSPORA PARASITICA 1) and ROQ1 (RECOGNITION OF XopQ 1) from *A. thaliana* and *Nicotiana benthamiana*, respectively, induces the formation of homotetrameric complexes, stimulating TIR enzyme activity. The resistosome TIR enzyme, but also TIR-only proteins, produce a variety of nucleotide-based second messenger molecules (Horsefield *et al.*, 2019; Wan *et al.*, 2019; Huang *et al.*, 2022; Jia *et al.*, 2022; Yu *et al.*, 2022), some of which serve as ligands to activate the EDS1 protein family plus the signalling/helper CNLs ADR1 or NRG1 (Lapin *et al.*, 2019; Huang *et al.*, 2022; Jia *et al.*, 2022). ADR1 and NRG1 can also function as calcium ion-permeable channels (Jacob *et al.*, 2021) and, as such, disruption of Ca^{2+} homeostasis appears to be central in CNL and TNL resistosome signalling.

The polymorphic barley *Mildew locus A* (*Mla*) encodes allelic variants of CNLs (MLA NLRs), each conferring isolate-specific disease resistance to the barley powdery mildew fungus *Blumeria graminis* f. sp. *hordei* (*Bgh*) (Moseman and Schaller, 1960; Glawe, 2008; Seeholzer *et al.*, 2010; Maekawa *et al.*, 2019). Some barley MLAs and *Mla* homologues of other cereals confer additional resistance to isolates of unrelated fungal pathogens (Periyannan *et al.*, 2013; Mago *et al.*, 2015; Chen *et al.*, 2017; Bettgenhaeuser *et al.*, 2021; Brabham *et al.*, 2022, Preprint; Ortiz *et al.*, 2022). The *Bgh* effectors recognized by barley MLAs are known as AVR_A effectors (Jorgensen, 1994), and diversified variants that have escaped *Mla* recognition are designated as AVR_A-V variants (Lu *et al.*, 2016). To date, full-length structures of inactive or effector-activated MLAs are not available, but protein interaction assays suggest a direct interaction between at least some MLA NLRs and matching AVR_A effectors (Saur *et al.*, 2019a). Most amino acids under positive selection of *Mla* resistance specificities map to the predicted solvent-exposed sites of the LRR, suggesting that these serve as AVR_A contact residues (Seeholzer *et al.*, 2010; Maekawa *et al.*, 2019), but interaction between effectors and MLA LRR domain deletion constructs could not be shown. Most of the known *Bgh* AVR_A effectors are unrelated in sequence, but share a common fold reminiscent of RNases lacking catalytic residues (Bauer *et al.*, 2021).

Mla13 (GeneBank AF523683.1; Halterman and Wise, 2006) in barley confers resistance to most *Bgh* isolates, representing a global pathogen population because these avirulent isolates express AVR_{A13}-1/BLGH_02099 (Lu *et al.*, 2016; Saur *et al.*, 2019a). *AVR_{a13}-1/BLGH_02099* is polymorphic in the *Mla13*-virulent *Bgh* isolates CC52 and B103, and the resulting gene products are named AVR_{A13}-V1 and AVR_{A13}-V2, respectively (Lu *et al.*, 2016). AVR_{A13}-1 is directly recognized by MLA13 (GeneBank AF523683.1; Halterman and Wise, 2006), and AVR_{A13}-1, but not AVR_{A13}-V1 or AVR_{A13}-V2, induces MLA13-mediated cell death upon transient co-expression of the respective genes in barley protoplasts and heterologous *N. benthamiana* leaves. AVR_{A13}-V1 represents a truncated version of AVR_{A13}-1 and, after transient gene overexpression *in planta*, the AVR_{A13}-V1 protein is unstable and often not detectable. Not in agreement with the virulent pathotype of *Bgh* isolate B103 on *Mla13* barley or the inability of AVR_{A13}-V2 to activate MLA13 cell death, interaction assays *in planta* and in yeast indicated a stable association between AVR_{A13}-V2 and MLA13 (Saur *et al.*, 2019a).

Because receptor–effector interaction is commonly linked to receptor activation, we aimed here to investigate the seeming paradox of MLA13 inactivity despite stable AVR_{A13}-V2–MLA13 association. By applying proximity-dependent protein labelling (BioID), yeast two-hybrid (Y2H) interaction assays, and structural prediction (Alphafold2) in combination with *in planta* expression of AVR_{A13} effector variants, we demonstrate that a single surface-exposed amino acid at the C-terminus of AVR_{A13} effectors determines the association with and activation of MLA13. Our data also reveal that AVR_{A13}-V2 acts as a dominant-negative effector on MLA13-mediated cell death. This proposes that breakdown of *Mla13*-mediated resistance can be explained by *Bgh* isolates carrying dominant-negative AVR_{A13}-V2. We also demonstrate that amino acid exchanges in the MLA13 NB and LRR domains compromise effector binding. In turn, amino acid changes in the MLA13 CC domain predicted to disrupt cation channel activity do not affect MLA13-mediated cell death. Nevertheless, inhibition of Ca^{2+} and other cation channels by $LaCl_3$ impaired MLA13-mediated cell death of barley protoplasts. Collectively, these results provide insights and tools for understanding the conformational changes NLRs undergo during effector-mediated NLR resistosome activation.

Materials and methods

Plant and fungal materials and growth conditions

Golden Promise and near sssisogenic lines (NILs) of the barley cultivar Manchuria were grown at 19 °C, 70% relative humidity, and under a 16 h photoperiod. *Nicotiana benthamiana* plants were grown under standard greenhouse conditions with a 16 h photoperiod. Maintenance of *Bgh* isolates was carried out as described previously (Lu *et al.*, 2016).

Generation of expression constructs

For transient gene expression assays in *N. benthamiana* and barley protoplasts and for Y2H interaction studies, coding sequences of receptor and effector genes with or without stop codons were either synthesized as pDONR221 entry clones from GeneArt (Thermo Scientific) or were published previously (Saur *et al.*, 2019a). Respective genes were transferred from entry or donor vectors using the Gateway LR Clonase II (Thermo Fisher) into the expression vectors pIPKb002 (Himmelbach *et al.*, 2007), pGWB414, pGWB517 (Nakagawa *et al.*, 2007), pXCSG-GW-HA, pXCSG-GW-Myc, pXCSG-GW-mYFP (Garcia *et al.*, 2010), pAMpAT-GW-BirA-4Myc, pLexA-GW, or pB42AD-GW (Shen *et al.*, 2007) as indicated using LR Clonase II (Thermo Scientific).

Transient gene expression by Agrobacterium*-mediated transformation of* N. benthamiana *leaves*

Agrobacterium tumefaciens GV3101:pMP90K were freshly transformed with the respective constructs of interest and grown from single colonies in liquid Luria broth medium containing appropriate antibiotics for ~24 h at 28 °C to an OD_{600} not higher than 1.5. Bacterial cells were harvested by centrifugation at 2500 *g* for 15 min followed by resuspension in infiltration medium (10 mM MES, pH 5.6, 10 mM $MgCl_2$, and 200 μM acetosyringone) to a final OD_{600}=1. Cultures were incubated for 2–4 h at 28 °C with 180 rpm shaking before infiltration into leaves from 3- to 5-week-old *N. benthamiana* plants. For co-expression of multiple constructs, Agrobacteria carrying the genes of interest were mixed equally unless indicated otherwise. Cell death was assessed 1–5 d post-infiltration as indicated, and tissue for immunodetection analysis was harvested 1–2 d post-infiltration as indicated.

Protein extraction from N. benthamiana *leaf tissue for protein detection by immunoblotting*

Frozen leaf material was ground to a fine powder using pre-cooled adapters in a bead beater (Retsch) and thawed in cold plant protein extraction buffer [150 mM Tris–HCl, pH 7.5, 150 mM NaCl, 10 mM EDTA, 10% (v/v) glycerol, 5 mM DTT, 2% (v/v) plant protease inhibitor cocktail (Sigma), 1 mM phenylmethylsulfonyl fluoride (PMSF), and 0.5% (v/v) IGEPAL] at a ratio of 50 mg fresh tissue/150 μl of extraction buffer. Extracts were centrifuged twice at 15 000 *g* for 10 min at 4 °C. For SDS–PAGE, extracts were diluted 4:1 with 4× SDS loading buffer and heated to 85 °C for 10–15 min before again removing insoluble material by centrifugation at 15 000 *g* for 5 min. For pull-down of monomeric yellow fluorescent protein (mYFP)-tagged proteins, green fluorescent protein (GFP)-Trap-MA (Chromotek) beads were incubated in equilibration buffer (Saur *et al.*, 2015) for 1 h at 4 °C and subsequently mixed with 1 ml of protein extracts for 2–3 h at 4 °C with slow but constant rotation.

Then, conjugated GFP-Trap beads were washed five times in 1 ml of cold wash buffer (Saur *et al.*, 2015) at 4 °C before interacting proteins were stripped from the beads by boiling in 25 μl of 4× SDS loading buffer for 5 min. Samples were separated on 8–13% SDS–PAGE gels, blotted onto a polyvinylidene fluoride (PVDF) membrane, and probed with anti-GFP (abcam ab6556), anti-Myc (abcam ab9106), or anti-HA (Roche 3F10) followed by anti-rabbit IgG–horseradish peroxidase (HRP) (Santa Cruz Biotechnology sc-2313) or anti-rat IgG–HRP (abcam ab97057) secondary antibodies. Epitope-tagged proteins were detected by the HRP activity on SuperSignal West Femto Maximum Sensitivity Substrate (Thermo Fisher 34095) using a Gel Doc™ XR+ Gel Documentation System (Bio-Rad).

Proximity-dependent protein labelling of proteins transiently expressed in N. benthamiana *leaves*

Pull-down of biotinylated proteins was performed by following published protocols (Conlan *et al.*, 2018) with the alteration that free biotin was not removed before adding streptavidin to protein extracts. Instead, we infiltrated (Shi *et al.*, 2023) a 10 μM biotin solution to the plant tissue (instead of a 75 μM solution; Conlan *et al.*, 2018). We followed a sequence of infiltrations to minimize MLA-mediated cell death of *N. benthamiana* leaf tissue: *Agrobacterium tumefaciens* GV3101::pMP90K carrying *35S:Mla-4Myc* constructs were grown from glycerol stocks and infiltrated (day 1). At 24 h post-infiltration of the *Mla* constructs, Agrobacteria freshly transformed with *35S:AVR$_{a13}$-BirA-4Myc* constructs or the empty vector (EV) were infiltrated as indicated (day 2). Free biotin (10 μM) in infiltration buffer lacking acetosyringone was infiltrated at 24 h after the second infiltration and 48 h after the first infiltration (day 3). Tissue for streptavidin-based precipitation of biotinylated proteins was harvested 24 h post-infiltration of free biotin. Frozen leaf material was ground to a fine powder using pre-cooled adapters in a bead beater (Retsch) and thawed in cold plant denaturing extraction buffer [150 mM Tris–HCl, pH 7.5, 150 mM NaCl, 10 mM EDTA, 5% (v/v) glycerol, 5 mM DTT, 1% (v/v) plant protease inhibitor cocktail (Sigma), 1 mM NaF, 1 mM sodium orthovanadate, 1 mM PMSF, 1% Triton X-100, and 0.5 % (w/v) SDS] at a ratio of 300 mg fresh tissue/2 ml of denaturing extraction buffer. Extracts were incubated rotating at 4°C for 30 min before the removal of insoluble material by centrifugation at 21 000 *g* for 30 min at 4 °C. Streptavidin-coated Dynabeads (100 μl per sample, MyOne streptavidin C1, Thermo Fisher) were incubated in wash buffer [150 mM Tris–HCl, pH 7.5, 150 mM NaCl, 10 mM EDTA, 5% (v/v) glycerol, 1% (v/v) plant protease inhibitor cocktail (Sigma)] containing 1% BSA for 1 h at 4 °C and subsequently mixed with 2 ml of protein extracts for 3 h at 4 °C with slow but constant rotation. Then, conjugated streptavidin beads were washed four times in 1 ml of cold wash buffer before interacting proteins were stripped from the beads by heating to 85 °C for 10–15 min in 50 μl of 4× SDS loading buffer. From these 50 μl, a 30 μl aliquot was loaded on 9% SDS–PAGE gels. Proteins were blotted onto a PVDF membrane and probed with anti-Myc (abcam ab9106) followed by anti-rabbit IgG–HRP (Santa Cruz Biotechnology sc-2313) secondary antibodies. Myc-tagged proteins were detected by the HRP activity on SuperSignal West Femto Maximum Sensitivity Substrate (Thermo Fisher 34095) using a Gel Doc™ XR+ Gel Documentation System (Bio-Rad).

Transient gene expression and cell death assay in barley protoplasts

Assessment of protoplast cell death using a luciferase (LUC) activity as a proxy for cell viability was performed as described (Saur *et al.*, 2019b). Briefly, *Mla* cDNA and *AVR$_a$* cDNAs lacking the respective signal peptide were expressed from the *Zea mays* ubiquitin promotor in protoplasts isolated from barley cultivar Golden Promise, Manchuria CI 2330, and cultivar Manchuria *Mla13* NIL CI 16155. For this, the epidermis of the secondary (Golden Promise) or primary (Manchuria) leaves from 7- to 8-day-old plants was removed before leaves were immersed in the enzyme solution. A total volume of 30 μl of water containing the *LUC* reporter and other constructs was transfected as indicated into 300 μl of barley protoplasts at a concentration of 3.5×10^5 protoplasts ml^{-1} solution. Protoplasts were recovered in regeneration buffer supplemented with $LaCl_3$ as indicated. About 16 h after transfection, protoplasts were collected by centrifugation at 1000 *g*, the supernatant was discarded, and 200 μl of 2× cell culture lysis buffer were added (Promega, E1531). LUC activity was determined by mixing 50 μl of protoplast lysate with 50 μl of LUC substrate (Promega, E1501) in a white 96-well plate, and light emission was measured at 1 s per well using a microplate luminometer (Centro, LB960).

Protein extraction from barley protoplasts, and fusion protein detection by immunoblotting

To determine the effect of $LaCl_3$ treatment on AVR$_{A13}$ protein, for each $LaCl_3$ treatment, 300 μg of the *AVR$_{a13}$-V2-mYFP* effector construct or an EV was transfected into 3 ml of barley protoplasts cultivar Manchuria CI 2330 at a concentration of 5×10^5 protoplasts ml^{-1} solution. Protoplasts were recovered in regeneration buffer supplemented with the $LaCl_3$ to the final concentrations indicated. About 16 h post-transfection, protoplasts were collected by centrifugation at 1000 *g*, the supernatant was discarded, and protoplast pellets were frozen in liquid nitrogen. Total protein was extracted by the addition of 100 μl of cold plant protein extraction buffer [200 mM Tris–HCl, pH 7.5, 150 mM NaCl, 10 mM EDTA, 10% (v/v) glycerol, 12 mM DTT, 2% (v/v) plant protease inhibitor cocktail (Sigma), and 1% (v/v) IGEPAL] to each protoplast pellet. Extracts were centrifuged at 15 000 *g* for 5 min at 4 °C. For SDS–PAGE, extracts were diluted 4:1 with 4× SDS loading buffer and heated to 85 °C for 10–15 min before removing insoluble material by centrifugation at top speed for 5 min. Samples were separated by 10% SDS–PAGE, blotted onto a PVDF membrane, and probed with anti-GFP (Santa Cruz Biotechnology sc-8334 or abcam ab6556) followed by anti-rabbit IgG–HRP (Santa Cruz Biotechnology sc-2313) secondary antibodies. mYFP-tagged proteins were detected by the HRP activity on SuperSignal West Femto Maximum Sensitivity Substrate (Thermo Fisher 34095) using a Gel Doc™ XR+ Gel Documentation System (Bio-Rad).

Yeast two-hybrid assay and yeast protein extraction

NLR receptor gene variants were cloned into the pLexA-GW vector (Shen *et al.*, 2007) for expression with an N-terminal LexA-binding domain under the control of a constitutive ADH1 promoter (BD-NLR). Effector variants were cloned into pB42AD-GW (Shen *et al.*, 2007) for expression with an N-terminal B42 activation domain followed by the HA-tag under the control of an inducible GAL1 promoter (AD-AVR). Using the lithium acetate method (Gietz and Woods, 2002), bait and prey constructs were co-transformed into the yeast strain EGY4.8 p8op, and successful transformants were selected by colony growth on SD-UHW/Glu [2% (w/v) glucose, 0.139% (w/v) yeast synthetic drop-out medium pH 6 without uracil, histidine, tryptophan, 0.67% (w/v) BD Difco yeast nitrogen base, 2% (w/v) Bacto Agar]. Yeast transformants were grown to OD_{600}=1 in liquid SD-UHW/Glu before harvesting cells for drop-out of the log dilution series on SD-UHW/Gal/Raf mediu [SD-UHW without glucose but with 2% (w/v) galactose 1% (w/v) raffinose, with (–UHW) or without leucine (–UHWL)] and incubated for 1–2 weeks at 30 °C.

For protein detection, yeast strains were grown to OD_{600}=1 in SD-UHW/Gal/Raf liquid medium at 30 °C and 200 rpm shaking, and proteins were extracted using 200 mM NaOH (NaOH method) (Zhang *et al.*, 2011). Total protein samples were separated by 9% or 12%

SDS–PAGE, blotted onto a PVDF membrane, and probed with anti-HA (Merck, clone 3F10) or anti-LexA (Santa Cruz Biotechnology, sc7544) primary antibodies followed by anti-rat (Santa Cruz Biotechnology, sc2065) or anti-mouse IgG–HRP (Santa Cruz Biotechnology, sc2005) secondary antibodies as appropriate. HA and LexA fusion proteins were detected by HRP activity on SuperSignal West Femto Maximum Sensitivity Substrate (Thermo Fisher 34095) using a Gel Doc™ XR+ Gel Documentation System (Bio-Rad).

Results

The C-terminus of AVR$_{A13}$ effectors determines interaction with and activation of MLA13

The C-terminally located polymorphisms between genes encoding avirulent AVR$_{A13}$-1 effector and virulent AVR$_{A13}$-V1 or AVR$_{A13}$-V2 variants (Fig. 1A) indicate a role for the AVR$_{A13}$-1 C-terminus in the interaction with and activation of MLA13. Previously, no avirulence activity could be detected for AVR$_{A13}$-V1, but this could be attributed to its protein instability upon transient expression *in planta* (Lu *et al.*, 2016; Saur *et al.*, 2019a). Here we aimed to stabilize AVR$_{A13}$-V1 protein to retest the association patterns of the AVR$_{A13}$ variants with MLA13 *in planta*. To this end, we fused the three effector variants to a biotin ligase (BirA), and indeed this fusion allowed immunodetection of the AVR$_{A13}$-V1 at levels comparable with the other two variants in *N. benthamiana* leaves (Supplementary Fig. S1). We also confirmed the functionality of the tagged proteins by demonstrating MLA13-specified cell death induced by AVR$_{A13}$-1-BirA-4×Myc. In turn, AVR$_{A13}$-V1-BirA-4×Myc and AVR$_{A13}$-V2-BirA-4×Myc did not activate MLA13-specified cell death in these assays (Supplementary Fig. S1). We detected biotinylated MLA13, but not MLA1 or MLA7 protein, in samples expressing *Mla13-4Myc* together with *AVR$_{a13}$-1-BirA* or *AVR$_{a13}$-V2-BirA*, but not *AVR$_{a13}$-V1-BirA* after biotin treatment followed by a streptavidin pull-down (Supplementary Fig. S1B). Given that AVR$_{A13}$-V1 lacks the 42 C-terminal amino acids of AVR$_{A13}$-1 (Fig. 1A), the data provide experimental evidence that the C-terminal half of AVR$_{A13}$ is needed for the association and activation of the MLA13 receptor.

Both AVR$_{A13}$-1 and AVR$_{A13}$-V2 associate with MLA13, but only AVR$_{A13}$-1 activates MLA13-mediated cell death (Saur *et al.*, 2019a) (Supplementary Fig. S1A). To delineate the AVR$_{A13}$-1 amino acids required for MLA13 cell death activation, we generated a truncated AVR$_{A13}$-1 construct (AVR$_{A13}$-1$^{\Delta SPE}$) and four hybrid variants of AVR$_{A13}$-1 and AVR$_{A13}$-V2, which differ from AVR$_{A13}$-1$^{\Delta SPE}$ by one, two, three, and four C-terminal amino acids, respectively (Fig. 1A). We then measured cell death upon co-expression of *Mla13* with *AVR$_{a13}$-1*, *AVR$_{a13}$-1$^{\Delta SPE}$*, or the hybrid variants in *N. benthamiana* leaves (Fig. 1B, C). Cell death comparable with *Mla13*- and *AVR$_{a13}$-1*-expressing leaf areas was only detected upon co-expression of *Mla13* with *AVR$_{a13}$-1$^{\Delta SPE}$* (Fig. 1B). The data demonstrate that the replacement of serine with leucine at position 119 abrogated MLA13-mediated cell death in *N. benthamiana* (Fig. 1A and 1B).

MLA13 interacts more efficiently with AVR$_{A13}$-V2 than with AVR$_{A13}$-1, and this enhanced association correlates with the inability to induce MLA13-mediated cell death (Saur *et al.*, 2019a). We therefore tested the association of AVR$_{A13}$-1$^{\Delta SPE}$ and the AVR$_{A13}$-1/AVR$_{A13}$-V2 hybrid variants with MLA13. Protein stability of AVR$_{A13}$ hybrid variants varies *in planta*, which makes the assessment of quantitative differences difficult (Fig. 1C). We therefore used a Y2H assay drop-out series to evaluate putative quantitative differences. We fused *Mla* N-terminally to the *LexA*-binding domain sequence (*BD-Mla13*) and the *AVR$_{a13}$* variants to the *B42* activation domain (*AD-AVR$_{a13}$*) and determined yeast growth in the absence of leucine as a proxy for protein interaction. Yeasts co-expressing *BD-Mla13* with *AD-AVR$_{a13}$-1* and *AD-AVR$_{a13}$-1$^{\Delta SPE}$* grew less in the dilution series than yeasts carrying *AD-AVR$_{a13}$-V2* or any of the *AD-AVR$_{a13}$* hybrid constructs (Fig. 1D). No growth was detected when *BD-Mla13* was co-expressed with *AD-AVR$_{a13}$-V1* or when it was replaced by *BD-Mla1* (Fig. 1D; Supplementary Fig. S2). The data imply that L^{119} of AVR$_{A13}$-V2 (Fig. 1A) is responsible for the enhanced interaction with MLA13. The corresponding residue in AVR$_{A13}$-1 is a serine. We generated structural predictions of the AVR$_{A13}$ variants [lacking the respective signal peptides (SPs)] using AlphaFold2 (pLDDT$_{overall}$=89, pLDDT$_{L/S119}$ >80) and found that indeed both, L^{119} of AVR$_{A13}$-V2 ΔSP and S^{119} of AVR$_{A13}$-1 ΔSP appear to be surface-exposed in these structural models, suggesting that they are accessible for binding to MLA13 (Supplementary Fig. S2C).

AVR$_{A13}$-V2 can act as a dominant-negative effector on MLA13-mediated cell death

The enhanced association between MLA13 and AVR$_{A13}$-V2 could affect *Mla13* disease resistance and the activity of other MLA NLRs. To test this, we measured AVR$_A$-induced MLA-mediated cell death in the presence of AVR$_{A13}$-V2. Co-expression of *Mla13-4×Myc* with *AVR$_{a13}$-1-mYFP* and an EV in *N. benthamiana* leaves resulted in cell death within 50–72 h, and this response was not detectable when EV was exchanged for *AVR$_{a13}$-V2-mYFP* (Fig. 2A). We also tested whether *AVR$_{a13}$-V2-4×Myc* affects cell death mediated by *Mla1-3×HA* and *AVR$_{a1}$-mYFP* or by *Mla7-3×HA* and *AVR$_{a7}$-2-mYFP*. We assessed the severity of cell death on a scale from 0 to 3 and found that AVR$_{A13}$-1- and MLA13-mediated cell death was abrogated by the co-expression of AVR$_{A13}$-V2. In contrast, *Mla1* and *AVR$_{a1}$* or *Mla7* and *AVR$_{a7}$-2* were not affected by *AVR$_{a13}$-V2* (Fig. 2B). The specific inhibitory effect of *AVR$_{a13}$-V2* on the MLA13 receptor (Fig. 2B) is not due to low MLA13 or AVR$_{A13}$-1 protein stability in the *AVR$_{a13}$-V2*-expressing samples (Fig. 2C). Importantly, AVR$_{A13}$-V1 had no inhibitory effect on cell death mediated by co-expression of *Mla13* and *AVR$_{a13}$-1*, even when

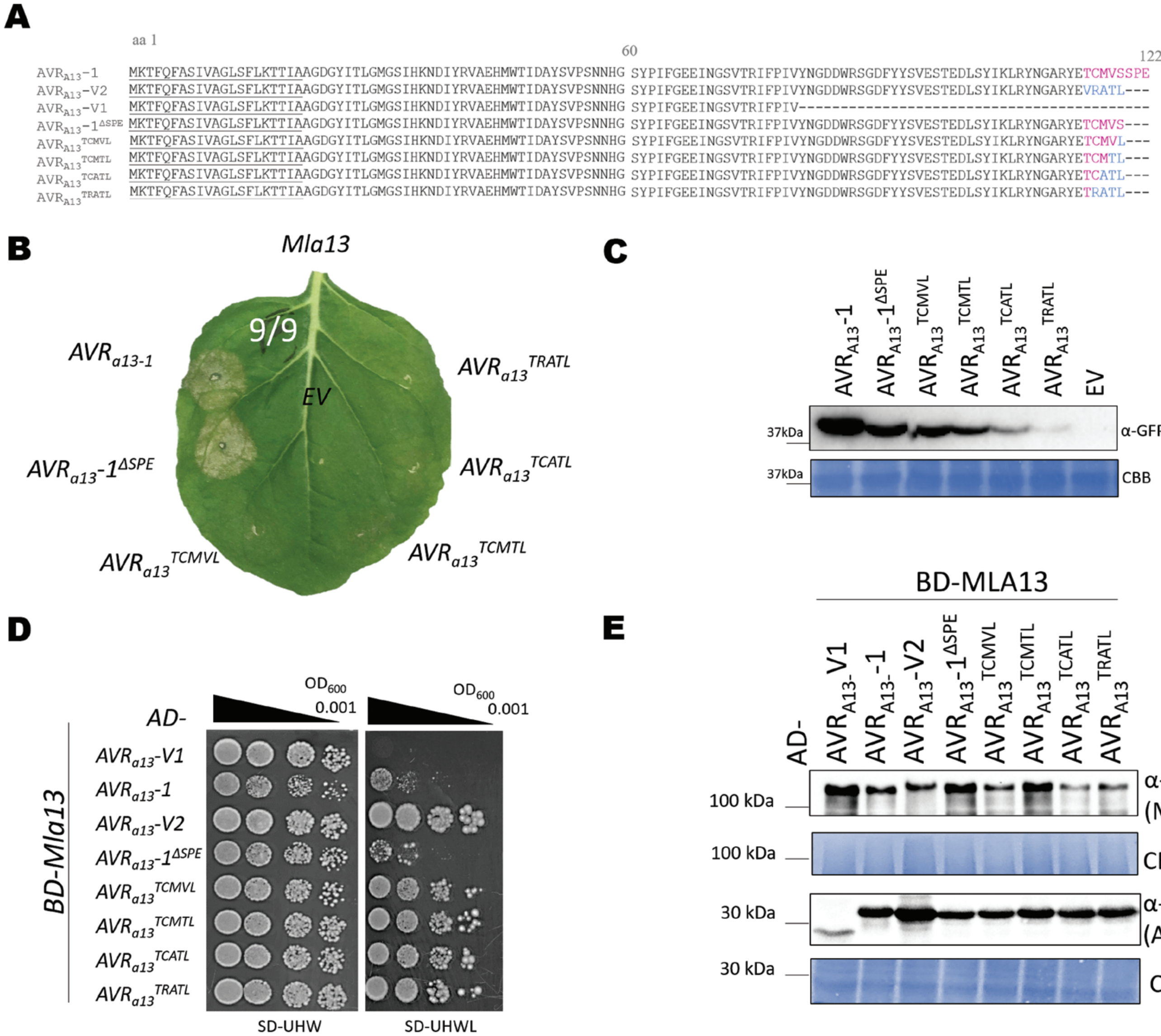

Fig. 1. The C-terminus of AVR_{A13} effectors controls interaction with and activation of MLA13. (A) Amino acid alignment of AVR_{A13} variants analysed for interaction with MLA13 and activation of MLA13-mediated cell death. Signal peptide (SP) residues are underlined; amino acids in blue and pink highlight the amino acid variation between AVR_{A13}-V2 and AVR_{A13}-1, respectively. (B and C) *Nicotiana benthamiana* leaves were transformed transiently with *35S:Mla13-4Myc* (pGWB517) with one of the *AVR_{a13}* variants lacking SPs cloned between the 35S promoter and a C-terminal *mYFP* sequence or empty vector (EV). (B) Cell death was determined 3 d post-transformation, and figures shown are representatives of at least nine independent leaves from at least three independent plants. (C) Protein stability of the AVR_{A13} variants fused to mYFP corresponding to constructs of (B). Leaf tissue was harvested 2 d post-infiltration. Total protein was extracted, separated by gel electrophoresis, and probed by anti-GFP. (D and E) Yeast cells were co-transformed with *Mla13* fused N-terminally to the *LexA*-binding domain (BD) sequence and *AVR_{a13}* variants lacking SPs fused N-terminally to the *B42* activation domain (AD) and 1×HA tag sequence as indicated. Growth of transformants was determined on selective growth medium containing raffinose and galactose as carbon sources but lacking uracil, histidine, and tryptophan (–UHW), and interaction of proteins was determined by leucine reporter activity reflected by growth of yeast on selective medium containing raffinose and galactose as carbon sources but lacking uracil, histidine, tryptophan, and leucine (–UHWL). Figures shown are representatives of at least three experiments, and pictures were taken 6–8 d after drop-out. (E) Protein levels of BD-MLA13 and AD-AVR_A variants corresponding to yeast of (D). Yeast transformants were grown in raffinose- and galactose-containing selective medium lacking uracil, tryptophan, and histidine to OD_{600}=1. Then, cells were harvested, total protein extracted, separated by gel electrophoresis, and western blots were probed with anti-LexA or anti-HA as indicated. CBB: Coomassie brilliant blue.

AVR_{A13}-V1 protein was stabilized by C-terminal fusion with the BirA tag (Supplementary Fig. S1C). Using a protoplast-based assay that relies on LUC activity as a proxy of cell viability (Saur *et al.*, 2019b), we also determined if $AVRA_{13}$-V2 inhibits MLA13 cell death in homologous barley. For this, we co-transfected protoplasts of the barley cultivar Golden Promise with the *LUC* reporter gene, *Mla1*, *Mla7*, or *Mla13*, and either EV or the matching *AVR_a* variant. In addition, EV

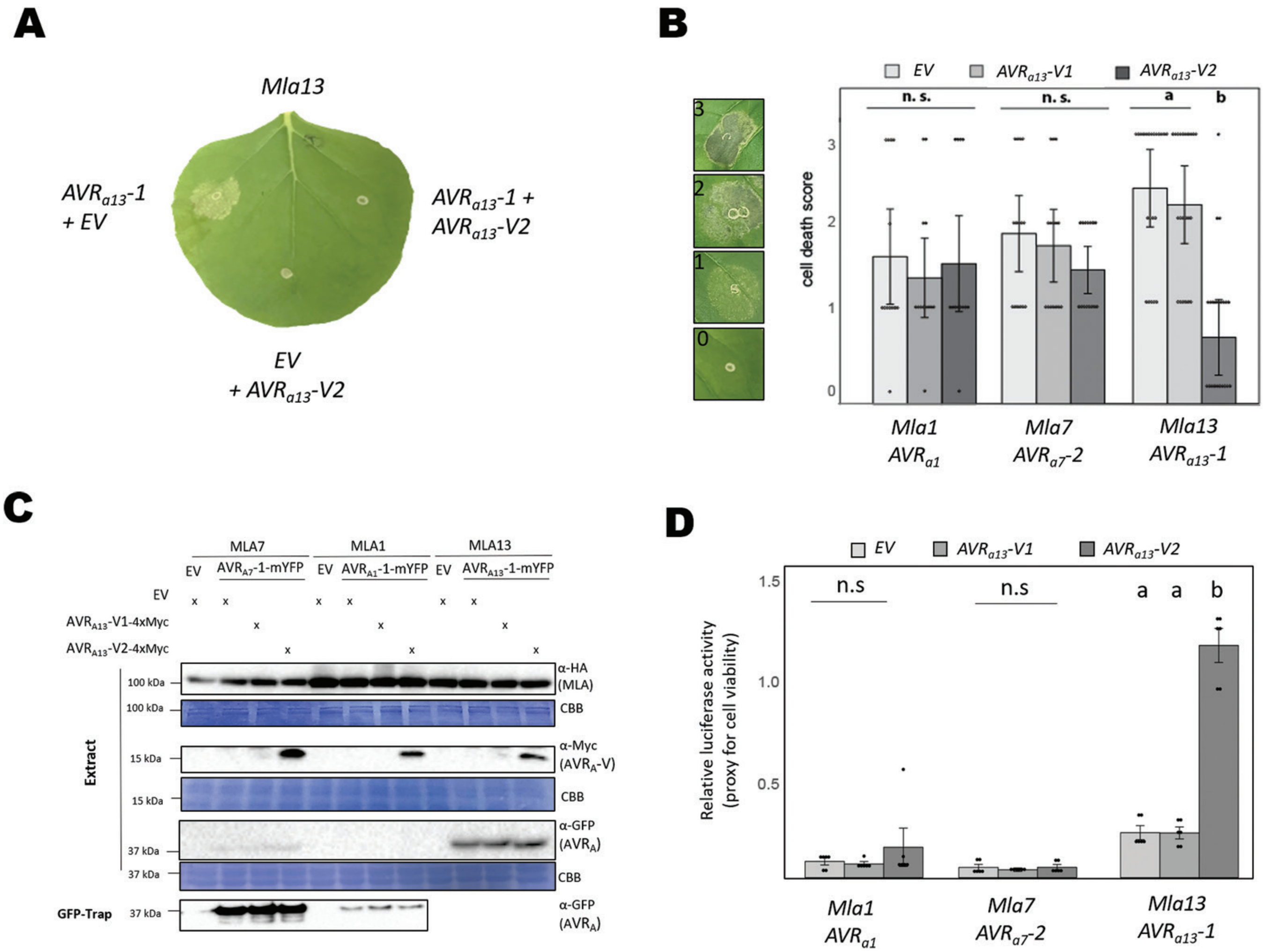

Fig. 2. AVR_{A13}-V2 can act as dominant-negative effector on MLA13. *Nicotiana benthamiana* leaves were co-transformed transiently with cDNAs of *Mla1* or *Mla7* or *MLA13* (pGWB vectors) with AVR_{a1}, AVR_{a7}*-2*, AVR_{a13}*-1*, or empty vector (EV) as indicated and either AVR_{a13}*-V1*, AVR_{A13}*-V2*, or EV fused to epitope tags as indicated. All constructs were expressed from the 35S promoter. (A and B) Cell death was determined 3–4 d post-transformation and (B) scored from 0 to 3 based on the cell death scale indicated. All values obtained in at least three independent experiments are indicated by dots; error bars=SE. Differences between samples were assessed by non-parametric Kruskal–Wallis and subsequent Dunn's tests for each MLA variant. Calculated *P*-values were as follows: *Mla1*, *P*=0.824; *Mla7*, *P*=0.551; and *Mla13*, *P*=1.00E-06. Samples marked by identical letters in the plots do not differ significantly (*P*<0.05) in the Tukey test for the corresponding MLA. (C) Protein levels corresponding to samples of (B). Leaf tissue was harvested 2 d post-infiltration. Total protein was extracted and recovered by GFP-Trap (AVR_{a1} and AVR_{a7}-2) separated by gel electrophoresis, and probed by anti-HA (MLAs), anti-Myc (AVR_{A13}-V2-4×Myc), or anti-GFP (AVR_{A1}–mYFP, AVR_{A7}-2–mYFP, and AVR_{A13}-1–mYFP) as indicated. CBB: Coomassie brilliant blue. (D) Barley protoplasts were transfected with *pUBQ:luciferase* (4.5 μg) and genes encoding *Mla1*, *Mla7*, or *Mla13* and either an EV (reference sample) or AVR_{a1}, AVR_{a7}*-2*, or AVR_{a13}*-1* lacking their respective signal peptides (SPs), respectively. Additionally, an EV or AVR_{a13}*-V1* or AVR_{a13}*-V2* lacking their respective SPs was co-expressed. The piPKb002 vector was used for all *Mla* and AVR_a constructs and, for each transfection, 9 μg of *Mla*-containing vector and 4.5 μg of each AVR_a-containing vector or EV were transfected. Luciferase activity was measured at 16 h post-transfection, and relative luciferase activity determined by setting the reference samples (*Mla*+EV) to 1. Differences between samples were assessed by non-parametric Kruskal–Wallis and subsequent Dunn tests for each MLA variant. Calculated *P*-values were as follows: *Mla1*: *P*=0.412; *Mla7*, *P*=0.683; and *Mla13*, *P*=1.9E-04. Samples marked by identical letters in the plots do not differ significantly (*P*<0.05) in the Dunn test for the corresponding MLA. n.s=not significant.

or plasmids encoding AVR_{a13}*-V1* or AVR_{a13}*-V2* genes were co-expressed. In comparison with the protoplasts transfected with *Mla* variants and EV plasmids, which served as control samples (relative luciferase activity=1), we detected strongly reduced LUC activity in the presence of the matching AVR_A variants (Fig. 2D). Co-transfection with genes encoding AVR_{a13}*-V1* instead of EV did not affect relative LUC activity. However, when EV was exchanged with AVR_{a13}*-V2*, the reduction of LUC activity induced by co-expression of AVR_{a13}-1 and *Mla13* was abolished but AVR_{a13}*-V2* expression had no significant effect on the cell death induced by samples expressing *Mla1* and AVR_{a1} or *Mla7* and AVR_{a7}*-2* (Fig. 2D). Together, or data suggest that AVR_{A13}-V2 has a dominant-negative effect on cell death activity specifically mediated by

MLA13 and that this is accompanied by enhanced interaction of the proteins.

Amino acid exchanges in the nucleotide-binding site of MLA13 compromise AVR$_{A13}$ effector binding

Previous reports on flax TNL L6 suggest an equilibrium between inactive and active NLR conformations in the absence of pathogen effectors, but that binding of the matching effector stabilizes the active NLR conformation (Bernoux *et al.*, 2016). We therefore hypothesized that avirulent AVR$_{A13}$-1 stabilizes the active ATP-bound oligomeric conformation of MLA13. Given that AVR$_{A13}$-V2 can inhibit MLA13-mediated cell death in co-expression assays (Fig. 2), we hypothesized that AVR$_{A13}$-V2 binds and stabilizes the inactive MLA13 receptor. To test this hypothesis, we applied the aforementioned Y2H approach to examine the interaction between naturally occurring AVR$_{A13}$ variants and MLA13 variants carrying mutations in the NB domain that render the MLA receptor inactive (P-loop mutants that cannot bind ADP or ATP at the NB domain) or autoactive (MHD mutant mimicking ATP binding at the NB domain) (Bai *et al.*, 2012). In the Y2H assay, yeast expressing BD-MLA13 together with AD-AVR$_{A13}$-1 or AD-AVR$_{A13}$-V2, but not AD-AVR$_{A13}$-V1, grew as expected. None of the yeast samples co-expressing BD-MLA13^{D502V} or BD-MLA13^{K207R} together with any AVR$_{A13}$ variants grew in the absence of leucine, although all proteins were stably detectable (Fig. 3A, B). We also wondered if similar results can be observed for other cereal CNLs, and therefore determined the interaction of autoactive Sr50 with AvrSr50. MLA13 and Sr50 are homologous genes and share 78% amino acid identity, whereas the effector genes are not related. Indeed, we observed similar results for the *Mla* homologue *Sr50*, although we detected growth of yeast expressing AD-AvrSr50 with the MHD variant Sr50^{D498V} fused N-terminally to the B42 BD. However, this interaction was consistently weaker when compared with samples co-transformed with wild-type Sr50. When AD-AvrSr50 was replaced by AD-AvrSr50$_{QCMJC}$, a variant lacking avirulence activity, no interaction was detected (Supplementary Fig. S3A, B).

AVR$_{A13}$-V2 binds specifically and strongly to wild-type MLA13 and can inhibit MLA13-specified cell death, suggesting a direct link between effector binding and cell death inhibition for this association. However, AVR$_{A13}$-V2 cannot bind autoactive MLA13^{D502V} in the Y2H assay (Fig. 3A) and we therefore speculate that it cannot inhibit MLA13^{D502V}-mediated cell death. Indeed, co-overexpression of *AVR$_{a13}$-V2* or *AVR$_{A13}$-V1* had no effect on MLA13^{D502V}-induced cell death observed as early as 2 d post-infiltration of the respective constructs in *N. benthamiana* leaves (Fig. 3C). Four to five days after infiltration of leaves with Agrobacteria carrying *35S:Mla13* at OD_{600}=1, we also detected effector-independent cell death mediated by wild-type MLA13 (MLA13 autoactivity). This average cell death score of 2 was significantly impaired in samples co-overexpressing *AVR$_{a13}$-V2* (average cell death score=0.5) but not *AVR$_{a13}$-V1*. Co-expression of *AVR$_{a13}$-V2* had no effect on the protein levels of any of the MLA13 variants used (Fig. 3D). Of note, cell death mediated by overexpression of the MLA13 CC domain (MLA13^{CC}, amino acids 1–160) was not affected by AVR$_{A13}$-V2 (Supplementary Fig. S3C, D).

Different affinities between MLA13 mutant variants and AVR$_{A13}$ effectors

The lack of AVR$_{A13}$ interaction with both inactive and active CNL MLA13 mutant variants was unexpected, as it contrasts with previous reports on flax TNL L6 and its matching effector AvrL567 (Bernoux *et al.*, 2016). We therefore investigated whether this lack of effector–receptor association could be generalized to other putatively inactive or autoactive MLA13 variants (Fig. 4A). We chose the MHD mutant variant H501G, whose autoactivity in MLA10 appears to be less pronounced than that of D502V (Bai *et al.*, 2012). Receptor autoactivity was also previously reported for MLA10^{F99E} (mutation in the CC domain) (Bai *et al.*, 2012). We also ssincluded the D284A mutant (mutation in the Walker A motif of the NB site, Fig. 4A) because the corresponding variant in the *A. thaliana* CNL RPM1 (RESISTANCE TO P. SYRINGAE PV MACULICOLA 1) leads to RPM1 autoactivity (Gao *et al.*, 2011). By substituting negatively charged residues in the first α-helix of MLA13 with alanine (MLA13^{D2A_E17A}), we aimed to generate an MLA13 resistosome that is structurally intact but impaired in immune signalling *via* Ca^{2+} influx (Wang *et al.*, 2019a, b; Bi *et al.*, 2021). This hypothesis is based on the observation that the replacement of negatively charged amino acids in the ZAR1 α1-helix abrogates Ca^{2+} influx and impairs cell death activity and ZAR1 disease resistance, but not formation and membrane association of the ZAR1 resistosome (Wang *et al.*, 2019a, b; Bi *et al.*, 2021). The S902F_F935I substitutions affect residues in the 14th and 15th LRRs of MLA13 (Fig. 4A), and the corresponding receptor is not expected to detect AVR$_{A13}$-1 as it is encoded by the barley line SxGP DH-47 (cross of cultivars SusPtrit and Golden Promise), which is fully susceptible to *Bgh* isolates carrying avirulent *AVR$_{a13}$* (Bettgenhaeuser *et al.*, 2021). We first tested our assumption that the MLA13 mutants exhibit altered cell death activities (inactive/autoactive). We expressed the corresponding gene constructs in *N. benthamiana* leaves and determined cell death in the presence and absence of AVR$_{A13}$-1. As reported for other MLA variants (Bai *et al.*, 2012), MLA13^{H501G} and MLA13^{F99E} showed effector-independent cell death activity in this assay. MLA13^{D284A} and SusPtritis MLA13^{S902F_F935I} receptor variants are unable to trigger host cell death when expressed together with *AVR$_{a13}$-1*. In turn, expression of MLA13^{D2A_E17A}, which is thought to be impaired in Ca^{2+} and cell death signalling (Bi *et al.*, 2021), resulted in effector-independent cell death in *N. benthamiana* leaves within 2 d post-infiltration (Fig. 4B). All MLA13 variants are detectable as fusion proteins (Fig. 4C).

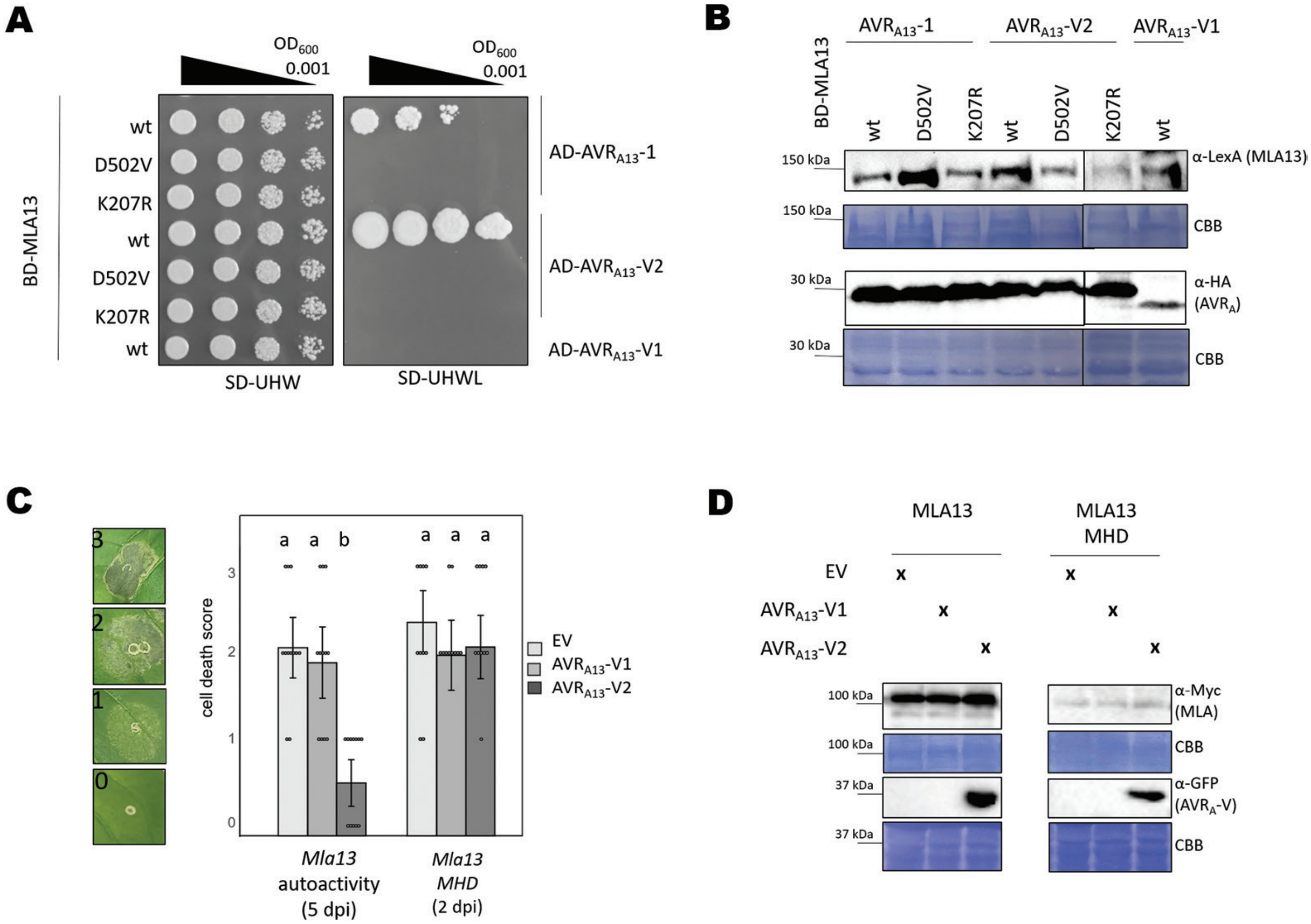

Fig. 3. Amino acid exchanges in the nucleotide-binding site of MLA13 compromise AVR_{A13} effector binding. (A, B) Yeast cells were co-transformed with *Mla13* wild type (wt) or mutant variants *Mla13*^{D502V} (MHD) or *Mla13 K207R* (P-loop) fused N-terminally to the *LexA*-binding domain (BD) sequence and *AVR*$_{a13}$ variants lacking SPs fused N-terminally to the *B42* activation domain (AD) and *1×HA* tag sequence as indicated. (A) Growth of transformants was determined on selective growth medium containing raffinose and galactose as carbon sources but lacking uracil, histidine, and tryptophan (–UHW), and interaction of proteins was determined by leucine reporter activity reflected by growth of yeast on selective medium containing raffinose and galactose as carbon sources, but lacking uracil, histidine, tryptophan, and leucine (–UHWL). Figures shown are representatives of at least three experiments, and pictures were taken 6–8 d after drop-out. (B) Protein levels of BD-MLA13 variants and AD-AVR_A variants corresponding to yeast of (A). Yeast transformants were grown in raffinose- and galactose-containing selective medium lacking uracil, tryptophan, and histidine to OD_{600}=1. Cells were harvested, total protein extracted, separated by gel electrophoresis, and western blots were probed with anti-LexA or anti-HA as indicated. (C and D) *Nicotiana benthamiana* leaves were co-transformed transiently with cDNAs of *AVR*$_{a13}$*-V1*, *AVR*$_{a13}$*-V2*, or empty vector (EV) together with constructs encoding either MLA13 or MLA13^{D502V} (pAM-PAT vector) as indicated and under the control of the 35S promoter sequence at a 2:1 ratio. (C) Cell death was determined 2 d (MLA13 MHD) to 5 d (MLA13) post-transformation and scored from 0 to 3 based on the cell death scale indicated. All values obtained in at least three independent experiments are indicated by dots;| error bars=SD. Differences between samples were assessed by non-parametric Kruskal–Wallis and subsequent Dunn's tests for each MLA variant. Calculated *P*-values were as follows: MLA13, *P*=5E-05; MLA13 MHD, *P*=0.078. Samples marked by identical letters in the plots did not differ significantly (*P*<0.05) in the Dunn test for the corresponding MLA. (D) Protein levels corresponding to samples of (C). Leaf tissue was harvested 36 h post-infiltration. Total protein was extracted, separated by gel electrophoresis, and probed by anti-Myc (MLAs) or anti-GFP (AVR_{A13}-V2) western blotting as indicated. CBB: Coomassie brilliant blue.

We next determined the ability of AVR_{A13}-V2 to bind the aforementioned MLA13 variants in a Y2H assay. Again, MLA13^{D502V} and MLA13^{K207R} variants served as negative controls. Yeast samples expressing *AD_AVR*$_{a13}$*-V2* together with wild-type *BD-Mla13* grew to a dilution of OD_{600}=0.001 quantitatively less when wild-type MLA13 was replaced with MLA13^{D2A_E17A} or MLA13^{F99E}. Samples transformed with *AD_AVR*$_{a13}$*-V2* and MLA13^{D284A}, MLA13^{K207R}, or MLA13^{S902F_F935I} showed no growth in the absence of leucine (Fig. 4D) although these MLA13 variants are stably expressed in yeast (Fig. 4E). The MLA F^{99} residue is not conserved in other CNLs and, therefore, the currently available CNL resistosome structures of ZAR1 and Sr35 cannot give functional insight into the role of this residue. However, the ZAR1 resistosome structures postulate that upon ligand binding, the release of the α1-helix in CNLs is an important conformational

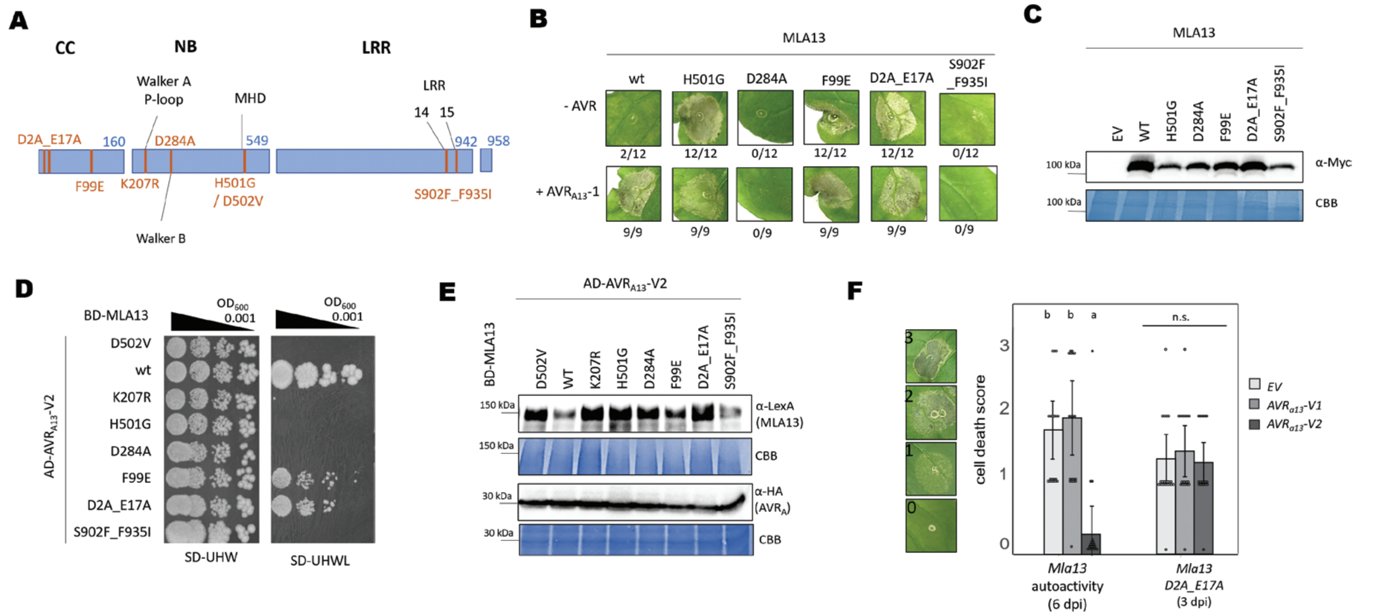

Fig. 4. Amino acid exchanges in the coiled-coil (CC) domain de-regulate MLA13 autoinhibition. (A) Amino acid changes in MLA13 mutant variants. The D2A_E17A and the F99E variants encode changes in the MLA13 CC domain, which spans from amino acid 1 to 160. The K207R, D284A, D502V, and H501G variants encode changes in the nucleotide-binding site (NB, amino acids 161– 549). The S902F_F935I variant affects the leucine-rich repeats (LRRs, amino acids 550–942) which are followed by a short C-terminal amino acid sequence. (B and C) *Nicotiana benthamiana* leaves were transformed transiently with cDNAs of one of the *Mla13* variants as indicated (pGWB517 vector) either with or without AVR_{a13}*-1* lacking SPs and fused C-terminally to an *mYFP* sequence. All constructs are under the control of the 35S promotor. (B) Cell death was determined 3 d post-transformation; $n \geq 9$. (C) Protein stability of the MLA variants fused to 4×Myc corresponding to constructs of (B). Leaf tissue was harvested 2 d post-infiltration. Total protein was extracted, separated by gel electrophoresis, and probed by anti-Myc western blotting as indicated. (D and E) Yeast cells were co-transformed with *Mla13* variants fused N-terminally to the *LexA*-binding domain (BD) sequence and AVR_{a13}-V2 lacking SPs fused N-terminally to the *B42* activation domain (AD) and *1×HA* tag sequence as indicated. Growth of transformants was determined on selective growth medium containing raffinose and galactose as carbon sources but lacking uracil, histidine, and tryptophan (–UHW), and interaction of proteins was determined by leucine reporter activity reflected by growth of yeast on selective medium containing raffinose and galactose as carbon sources but lacking uracil, histidine, tryptophan, and leucine (–UHWL). Figures shown are representatives of at least three experiments, and pictures were taken 6–8 d after drop-out. (E) Protein levels of BD-MLA13 variants and AD-AVR_{A13}-V2 corresponding to yeast of (D). Yeast transformants were grown in raffinose- and galactose-containing selective medium lacking uracil, tryptophan, and histidine to OD_{600}=1. Then, cells were harvested, total protein extracted, separated by gel electrophoresis, and western blots were probed with anti-LexA or anti-HA as indicated. CBB: Coomassie brilliant blue. (F) *N. benthamiana* leaves were co-transformed transiently with cDNAs of AVR_{a13}*-V1*, AVR_{a13}*-V2*, or empty vector (EV) together with constructs encoding the MLA13 variant as indicated and under the control of the 35S promoter sequence at a 2:1 ratio. Cell death was determined based on the cell death scale indicated. All values obtained in at least two independent experiments are indicated by dots, error bars=SD. Differences between samples were assessed by non-parametric Kruskal–Wallis and subsequent Dunn's tests for each MLA variant. Calculated *P*-values were as follows: MLA13, *P*=9.38E-07; $MLA13^{D2A\_E17A}$, *P*=0.77. n.s.=no significant difference.

change that occurs immediately before resistosome formation (Wang *et al.*, 2019a, b). We thus speculate that the autoactivity of $MLA13^{D2A\_E17A}$ is a result of mutation-induced α1-helix release. If this is the case, then this autoactivity cannot be inhibited by the dominant-negative AVR_{A13}-V2 ligand. Co-expression of AVR_{a13}*-V2-mYFP* with $MLA13^{D2A\_E17A}$ in *N. benthamiana* leaves indeed had no impact on the average cell death score, whereas autoactivity of wild-type MLA13 was again inhibited by co-expression of AVR_{a13}*-V2-mYFP* (Fig. 4F).

Activity of cation channels is required for MLA13 cell death

In ZAR1, the negatively charged residues on the inner lining of the ZAR1 resistosome funnel are required for Ca^{2+} channel activity, and substitutions of these amino acids impaired ZAR1 signalling (Wang *et al.*, 2019b; Bi *et al.*, 2021). In contrast, such substitutions in Sr35 had no effect on cell death or channel activity (Förderer *et al.*, 2022a), and the same appears to be true for $MLA13^{D2A\_E17A}$ (Fig. 4B). The data suggest that MLA13 does not require the negatively charged amino acids of the α1-helix in the CC domain for cell death signalling. We thus aimed to determine whether Ca^{2+} channel activity is needed for MLA13-mediated cell death in barley by applying the potent cation channel inhibitor $LaCl_3$. Toward this end, we expressed a LUC reporter together with AVR_{a13}*-1* in barley mesophyll protoplasts, prepared from the *Mla13*-containing near-isogenic backcross line Manchuria (CI 16155), and measured LUC activity as an indicator of protoplast viability. Protoplasts from the cultivar Manchuria (CI 2330), which lack *Mla13*, served as control. With increasing $LaCl_3$ concentration, we observed a reduction in LUC activity by up to

50% of CI 2330 protoplasts (20 μM $LaCl_3$), suggesting a detrimental impact of $LaCl_3$ treatment on protoplast viability independent of *Mla13* or a reduction in LUC activity independent of cell death. Nonetheless, in the absence of $LaCl_3$, LUC activity is on average >70% lower in *Mla13* protoplasts transfected with the *AVR_{a13}-1* construct than in protoplasts that do not express *Mla13* (Fig. 5A). This difference in LUC activity between the two samples diminishes with increasing $LaCl_3$ concentration and is no longer significant in samples treated with 10 μM $LaCl_3$. Although LUC activity decreases with increasing $LaCl_3$ concentrations, $LaCl_3$ treatment does not affect AVR_{A13}-1 protein stability in protoplasts of the cultivar Manchuria (Fig. 5B). Although we cannot exclude that $LaCl_3$ treatment affects *Mla13* expression in barley line CI 16155, our data show that blocking the function of cation channels by $LaCl_3$ compromises MLA13-mediated cell death in barley leaf protoplasts.

Discussion

Functional studies of effector recognition by NLRs are important not only for a better understanding of plant disease resistance but also for dissecting the mechanisms pathogens employ to overcome NLR-mediated resistance. To address both aspects, we studied MLA13-mediated recognition of the barley powdery mildew $AVRa_{A13}$ effector family with a particular focus on AVR_{A13}-V2, which originated from a *Bgh* isolate that has overcome *Mla13* resistance. We demonstrate that AVR_{A13}-V2 can act as a dominant-negative effector on MLA13-mediated cell death. The concept of effector proteins suppressing the recognition of another effector by NLRs or other classes of resistance proteins has been described previously for multiple independent interactions. For example, the *Leptosphaeria maculans* effector AvrLm4-7 masks AvrLm3 recognition by the Arabidopsis TIR-containing protein RLM3 (Plissonneau *et al.*, 2016), and the wheat powdery mildew-encoded *suppressor of avirulence SvrPm3a1/f1* gene negatively acts on wheat *Pm3*, which encode CNLs that recognize AvrPm3 variants from the wheat powdery mildew pathogen (Bourras *et al.*, 2015). Similarly, *Phytophthora infestans* effector IPI-O1 (Avrblb1) elicits Rpi-blb1 resistance in wild potato, while the effector variant IPI-O4, that can also bind Rpi-blb1, functions to suppress this resistance elicitation (Chen *et al.*, 2012). Our data demonstrate that the inhibitory function of AVR_{A13}-V2 on MLA13-mediated cell death is linked to enhanced association between AVR_{A13}-V2 and MLA13, and this in turn can prevent the detection of AVR_{A13}-1 by MLA13.

Mutations in the NB site of MLA13 abrogate association with its matching effector

The residues of the MLA LRR domains, which are under positive selection, may serve as effector contact residues (Seeholzer *et al.*, 2010; Maekawa *et al.*, 2019). Residues S^{902} and P^{935} in the 14th and 15th LRRs of MLA13 are exchanged for other amino acids in MLA13 encoded by a cultivar that has lost *Mla13* resistance function (Bettgenhaeuser *et al.*, 2021), and we showed here that these amino acid exchanges abrogate effector binding and activation of MLA13 (Fig. 4). Importantly, however, our data show that an intact, ADP-bound MLA13 receptor conformation is required for

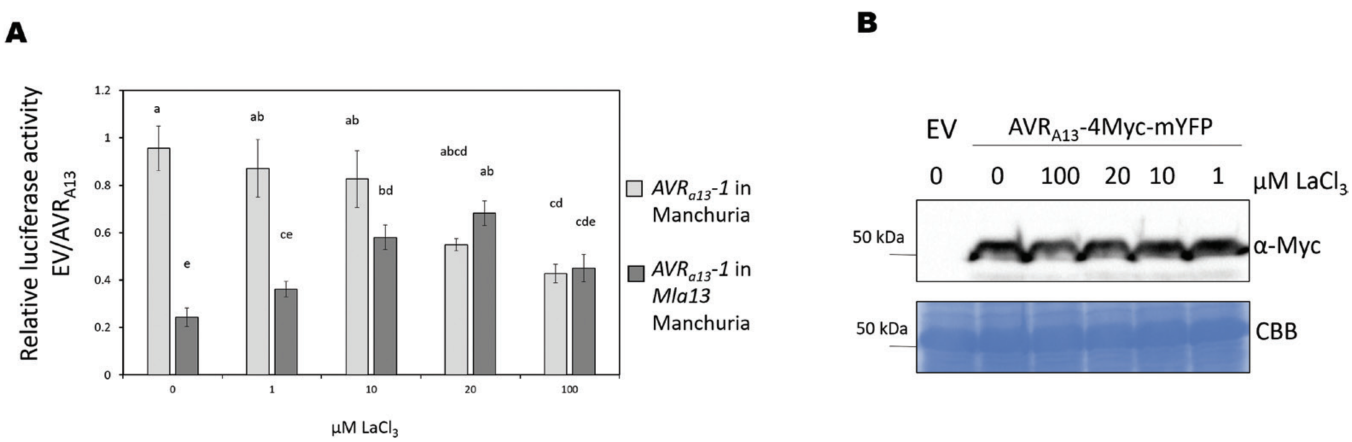

Fig. 5. Calcium channel activity is required for *Mla13*-mediated cell death in barley. (A) Barley protoplasts of lines CI 16155 (cultivar Manchuria *Mla13*) and CI2330 (Manchuria) were transfected with *pUBQ:luciferase* (6 μg) and piPKb002 containing *AVR_{a13}-1* cDNA without signal peptide (5 μg) or a piPKb002 empty vector control (5 μg) and recovered in the presence of $LaCl_3$ at the concentrations indicated. Luciferase activity was determined 16 h post-transfection/addition of $LaCl_3$ as a proxy for cell death and normalized against the respective EV sample. Error bars=SE. Differences between samples were assessed using non-parametric Kruskal–Wallis and subsequent Dunn's post-hoc tests. *P*=6.179e-10. Samples marked by identical letters in the plot did not differ significantly (*P*<0.05) in Dunn's test. (B) Protoplasts derived from cultivar Manchuria CI2330 leaves transfected with *pZmUBQ:AVR_{a13}-1-mYFP* were harvested 16 h post-transfection/$LaCl_3$ treatment. Total protein was extracted, separated by gel electrophoresis, and western blots were probed with anti-GFP. CBB: Coomassie brilliant blue.

efficient effector–receptor association in yeast. Disruption of this intact conformation by mutations in the NB site of MLA13, which result in the so-called 'MHD' (mimicking ATP binding) and 'P-loop' (no binding of ADP/ATP) receptor versions (Supplementary Fig. S4) fully abrogated interaction with the matching AVR_{A13} effector variants in Y2H assay, probably because of spatial hindrance. One possible explanation for this hindrance is that residues of the MLA13 NB domain are engaged in the formation of an effector-accessible conformation of the MLA LRR domain; that is, a site of effector entry (Förderer *et al.*, 2022b) only provided by ADP-bound MLA13 (Supplementary Fig. S4). At this effector entry site of ADP-bound MLA13, the MLA13 NB domain may transiently contact the AVR_{A13} ligand, and this contact may be required for the steric clash that dislocates the NB domain for ADP to ATP exchange. In fact, one intermediate state structure of the ADP-bound ZAR1 monomer bound to the activating PBL2 ligand (PDB 6j5v) implies contact between the ZAR1 NB domain and the PBL2 ligand ultimately before the steric clash that allows effector-mediated ZAR1 resistosome formation, although association between these contact-forming residues cannot be detected in the active, ATP-bound ZAR1 resistosome (Wang *et al.*, 2019b). An alternative hypothesis of our findings is a transient association between AVR_{A13} and MLA13, implying that conformational changes of MLA13 to the active oligomeric ATP-bound state lead to dislodging of AVR_{A13} effectors from the resistosome complex. However, this model is in contrast to the observation of all active NLR resistosome structures available to date, where each NLR monomer stably binds one activating ligand. The autoactive wheat CNL $Sr50^{MHD}$ mutant was also impaired in AvrSr50 association when compared with wild-type Sr50 (Supplementary Fig. S3), but our data contrast with the example of enhanced association between the flax TNL L6 MHD version and its matching effector (Bernoux *et al.*, 2016). Also, a disrupted P-loop does not hinder the CNL Rpi-amr3 binding to the matching *Phytophthora* effector in co-immunoprecipitation assays (Ahn *et al.*, 2023). We therefore suggest different requirements for NB domains at the site of effector entry for individual NLRs. However, we cannot entirely exclude that this difference may be due to the initiation of yeast cell death upon expression of CNL^{MHD}, whereas TNL^{MHD} variants cannot induce cell death in yeast. However, the $MLA13^{MHD}$ and $Sr50^{MHD}$ protein levels are as stable as those of wild-type receptors, and yeast growth in the presence of leucine is similar between yeasts expressing the wild type and the MHD variants (Fig. 3B; Supplementary Fig. S3D).

Blocking TNL ROQ1-mediated cell death signalling in *eds1* knockout lines in *N. benthamiana* was important for purification of the tetrameric ROQ1–effector resistosome (Martin *et al.*, 2020). We and others have previously attempted to detect interaction between CNLs and their matching effector *in planta* by using NLR P-loop mutants to prevent NLR-mediated cell death. Our data here showing that MLA13 P-loop variants have lost the ability to bind matching effectors explains why these attempts were unsuccessful.

Amino acid exchanges in the MLA13 α1-helix deregulate autoinhibition but not Ca^{2+}-dependent MLA13 cell death function

Negatively charged residues in the α1-helix of NLR CC domains are thought to be required for Ca^{2+} channel activity of CNL resistosomes (Förderer *et al.*, 2022b). This was inferred from the observation that replacement of these residues with alanine abrogated ZAR1 Ca^{2+} channel activity and ZAR1-mediated resistance. We observed that the negatively charged residues $MLA13^{D2}$ and $MLA13^{E17}$ in the α1-helix are not required for MLA13-mediated cell death and that these amino acid exchanges instead lead to effector-independent cell death in *N. benthamiana* (Fig. 4). We speculate that in the absence of a matching effector, these negatively charged amino acids in MLA13 are required for burying the α1-helix and that this autorepression malfunctions in $MLA13^{D2A\_E17A}$ (i.e. the α1-helix is exposed and available for oligomerization; Supplementary Fig. S4). However, our data cannot clarify whether the hypothetical autoactive α1-helix conformation of $MLA13^{D2A\_E17A}$ allows the exchange of ADP to ATP or whether an ADP-bound NB domain is even capable of forming a functional oligomer (Supplementary Fig. S4). Notably, the MLA residues L^{15} and L^{19}, which are predicted to be essential for MLA membrane association by analogy with the ZAR1 resistosome, were previously shown to abrogate cell death activity (Bai *et al.*, 2012), and the same was demonstrated for Sr35 (Förderer *et al.*, 2022a).

The cell death autoactivity of $MLA13^{D2A\_E17A}$ contrasts with similar ZAR1 mutants, which abolish cell death, but the data are comparable with results reported for other CNLs, including wheat Sr35 (Adachi *et al.*, 2019; Förderer *et al.*, 2022a). Despite these differences, we demonstrate that MLA13-dependent and AVR_{A13}-triggered cell death activity in barley protoplasts is impaired in the presence of the cation channel inhibitor $LaCl_3$ (Fig. 5), suggesting that cation transport across plant cell membranes by a putative MLA13 channel and/or other cation channels is also an important biochemical activity of the deduced MLA13 resistosome. Although the exact mechanism for cation transport in the putative MLA13 resistosome remains to be determined, our data align with reports on other CNLs that confer calcium channel-dependent cell death (Grant *et al.*, 2000; Förderer *et al.*, 2022a), and underline that perturbation of Ca^{2+} homeostasis is a fundamental component of both TNL- and CNL-mediated cell death in plants (Jubic *et al.*, 2019; Jacob *et al.*, 2021; Saur *et al.*, 2021; Förderer *et al.*, 2022a).

A single effector residue can disrupt NLR activation

As LRR domains have the potential to bind a variety of proteinaceous ligands, engineering the LRR domains of NLRs to bind pathogen effectors that are not recognized by the natural immune system appears to be an attractive strategy for controlling plant diseases. Our data demonstrate that ligand binding *per se* is not sufficient for NLR activation and that the exchange of a single, potentially surface-exposed residue (S119L exchange between $AVR_{A13}{}^{\Delta SPE}$ and $AVR_{A13}{}^{TCML}$) can abrogate NLR activation *in planta* despite enhanced interaction of MLA13 and L^{119}-containing $AVR_{A13}{}^{TCML}$ in Y2H assays (Fig. 1). L^{119} may mediate direct contact with MLA13 or change the conformation of the AVR_{A13} for enhanced interaction with MLA13. The dominant-acting interaction may directly allow AVR_{A13}-V2 to outcompete all AVR_{A13}-1 effectors for association with MLA13 and subsequent receptor activation. Alternatively, AVR_{A13}-V2 sequestration of some MLA13 monomers might be sufficient to disrupt putative MLA13 resistosome formation if a threshold of ligand-activated CNLs must be available for CNL resistosomes to be formed (Förderer *et al.*, 2022b). The possibility that AVR_{A13}-V2 sequesters AVR_{A13}-1 from activation of MLA13 appears less likely because AVR_{A13}-V2 can also inhibit MLA13 autoactivity (Fig. 2). The contact residues responsible for the activation of MLA13 by AVR_{A13} are likely to be unique, despite the overall structural similarity of AVR_{A} effectors and allelic, highly sequence-similar MLA receptors (Seeholzer *et al.*, 2010; Bauer *et al.*, 2021). This appears to be also true for the residues of AVR_{A13}-V2 that mediate MLA13 interaction, as neither the enhanced interaction, nor the dominant-negative effect of AVR_{A13}-V2 was detected when MLA13 was replaced by the highly sequence-similar MLA1 or MLA7 NLRs. The overall high sequence and predicted structural identity between AVR_{A13}-1 and AVR_{A13}-V2, as well as the identification of a single residue, L^{119} of AVR_{A13}-V2, as the main driver of enhanced MLA13 interaction, suggest that the binding surfaces to the MLA13 receptor overlap. However, our data imply that AVR_{A13}-V2 locks MLA13 into an inactive, effector-bound state by preventing the receptor from transitioning to one of the conformational changes downstream of effector binding (Supplementary Fig. S5). AVR_{A13}-V2 cannot inhibit cell death signalling of MLA13 constitutive gain-of-function mutants with amino acid replacements in the CC domain despite interaction with $MLA13^{D2A\_E17A}$ (Fig. 4D). We therefore suggest that the inhibitory function of AVR_{A13}-V2, mediated by L^{119}, affects conformational changes that take place before the release of the MLA13 α1-helix; that is, AVR_{A13}-V2 binding to MLA13 either fails to induce an interdomain steric clash in the receptor or blocks the transition to the steric clash-mediated open conformation, which allows exchange of ADP to ATP in the NB site of MLA13 (Supplementary Fig. S5). Alternatively, AVR_{A13}-V2 binding to MLA13 induces a steric clash, but AVR_{A13}-V2 association inhibits the release of the α1-helix from autorepression. As MLA13 MHD mutants are generally inaccessible to effector binding in Y2H assay (including binding to avirulent AVR_{A13}-1, Fig. 3), our data cannot clarify whether the loss of inhibitory function of AVR_{A13}-V2 on MLA13 cell death takes place before or after ADP exchange to ATP in wild-type MLA13. Collectively, we demonstrate that the stable interaction between AVR_{A13}-V2 and inactive MLA13 has the potential to define distinct conformations of intermediate states of CNL receptors. This knowledge is currently largely elusive for both animal and plant NLRs. Understanding such conformations will help ensure that future synthetic NLRs do not become locked into intermediate non-functional states.

Role of AVR_{A13}-V2 in the breakdown of Mla13 *resistance in the European* Bgh *population*

Evasion of NLR-mediated pathogen recognition is usually mediated by diversification of the pathogen's effector repertoire, including allelic variation of effector genes that results in abrogation of effector–NLR receptor associations. This model applies to the virulent variant AVR_{A13}-V1. However, AVR_{A13}-V2 not only interacts strongly with MLA13, but also inhibits MLA13 cell death signalling in a dominant manner (Fig. 2). This raises the possibility that *Bgh* AVR_{A13}-V2 facilitates dispersal of virulence in *Bgh* populations that are genetically avirulent on *Mla13*. In the European *Bgh* population, the virulence frequency on *Mla13* increased from 0.2% in the 1980s to as high as 60% in 1995 (Gacek, 1987; Jørgensen and Hovmøller, 1987; Hovmøller *et al.*, 2000), suggesting a major shift in genetic variation of $AVRa_{13}$ on a continental scale. In contrast, only 7% of *Bgh* isolates in a global strain collection carry virulent AVR_{A13} variants (Rsaliyev *et al.*, 2017; Saur *et al.*, 2019a). In addition, AVR_{a13}*/BGH_20990* has a very low frequency of non-synonymous polymorphisms in tested *Bgh* populations (0.9 non-synonymous single nucleotide polymorphisms/100 bp coding sequence), indicating an overall low genetic diversity of AVR_{a13} (Saur *et al.*, 2019a). Our data demonstrate a dominant-negative activity of AVR_{A13}-V2 on MLA13, therefore suggesting that the breakdown of *Mla13* resistance was caused by direct manipulation of the receptor activation mechanism rather than by evasion of MLA13 recognition.

Supplementary data

The following supplementary data are available at *JXB* online.

Fig. S1. Proximity-dependent protein labelling confirms the requirement of AVR_{A13} C-terminus for MLA13 interaction.

Fig. S2. Specificity control to Fig. 1D and structural prediction models

Fig. S3. Gain-of-function NLR mutants and their ability to bind matching avirulence effectors.

Fig. S4. Schematic model of MLA13 wild-type and mutant conformations.

Fig. S5. Schematic hypothetical models of MLA13 activation by *Bgh* AVR_{A13}-1 and inhibition by AVR_{A13}-V2, respectively.

Acknowledgements

We would like to thank Ksenia Krasileva for critical comments on the manuscript. Although the resulting crosses could not be assessed for *Bgh* infection due to loss of Mla13 resistance in control lines, we highly acknowledge the group of Matthew Moscou that crossed *Mla13* barley with *AVR_{a13}-V2* transgenic lines for assessing AVR_{A13}-V2-mediated inhibition of *Mla13* resistance.

Author contributions

EEC, MBS, TM, PSL, and IMLS: design; EEC, MBS, and IMLS: performing the experiments and data analysis; EEC, IMLS, and PSL: writing the paper with contributions from all authors.

Conflict of interest

No conflict of interest declared.

Funding

IMLS, TM, and PSL all acknowledge funding from the Deutsche Forschungsgemeinschaft (DFG, German Research Foundation) Collaborative Research Centre Project-ID 414786233 (SFB 1403) and support from the Cluster of Excellence on Plant Sciences (CEPLAS) funded by the DFG under Germany's Excellence Strategy—EXC 2048/1—Project ID: 390686111. This work was also funded by the DFG Emmy Noether Programme (SA 4093/1-1 to IMLS), the Daimler and Benz Foundation (IMLS), and the Max Planck Society (PSL).

Data availability

All relevant data are available within the paper and its supplementary data published online.

References

Adachi H, Contreras MP, Harant A, *et al*. 2019. An N-terminal motif in NLR immune receptors is functionally conserved across distantly related plant species. eLife **8**, e49956.

Ahn HK, Lin X, Olave-Achury AC, Derevnina L, Contreras MP, Kourelis J, Wu CH, Kamoun S, Jones JDG. 2023. Effector-dependent activation and oligomerization of plant NRC class helper NLRs by sensor NLR immune receptors Rpi-amr3 and Rpi-amr1. The EMBO Journal **42**, e111484.

Bai SW, Liu J, Chang C, *et al*. 2012. Structure–function analysis of barley NLR immune receptor MLA10 reveals its cell compartment specific activity in cell death and disease resistance. PLoS Pathogens **8**, e1002752.

Bauer S, Yu D, Lawson AW, Saur IM, Frantzeskakis L, Kracher B, Logemann E, Chai J, Maekawa T, Schulze-Lefert P. 2021. The leucine-rich repeats in allelic barley MLA immune receptors define specificity towards sequence-unrelated powdery mildew avirulence effectors with a predicted common RNase-like fold. PLoS Pathogens **17**, e1009223.

Bendahmane A, Farnham G, Moffett P, Baulcombe DC. 2002. Constitutive gain-of-function mutants in a nucleotide binding site-leucine rich repeat protein encoded at the Rx locus of potato. The Plant Journal **32**, 195–204.

Bernoux M, Burdett H, Williams SJ, *et al*. 2016. Comparative analysis of the flax immune receptors L6 and L7 suggests an equilibrium-based switch activation model. The Plant Cell **28**, 146–159.

Bernoux M, Ve T, Williams S, Warren C, Hatters D, Valkov E, Zhang XX, Ellis JG, Kobe B, Dodds PN. 2011. Structural and functional analysis of a plant resistance protein TIR domain reveals interfaces for self-association, signaling, and autoregulation. Cell Host & Microbe **9**, 200–211.

Bettgenhaeuser J, Hernández-Pinzón I, Dawson AM, *et al*. 2021. The barley immune receptor Mla recognizes multiple pathogens and contributes to host range dynamics. Nature Communications **12**, 6915.

Bi G, Su M, Li N, *et al*. 2021. The ZAR1 resistosome is a calcium-permeable channel triggering plant immune signaling. Cell **184**, 3528–3541.

Bourras S, McNally KE, Ben-David R, *et al*. 2015. Multiple avirulence loci and allele-specific effector recognition control the Pm3 race-specific resistance of wheat to powdery mildew. The Plant Cell **27**, 2991–3012.

Brabham HJ, Cruz DGD, Were V, *et al*. 2022. Barley MLA3 recognizes the host-specificity determinant PWL2 from rice blast (*Magnaporthe oryzae*). bioRxiv. doi:10.1101/2022.10.21.512921. [Preprint].

Burdett H, Bentham AR, Williams SJ, Dodds PN, Anderson PA, Banfield MJ, Kobe B. 2019. The plant 'Resistosome': structural insights into immune signaling. Cell Host & Microbe **26**, 193–201.

Cesari S. 2018. Multiple strategies for pathogen perception by plant immune receptors. New Phytologist **219**, 17–24.

Chen J, Upadhyaya NM, Ortiz D, *et al*. 2017. Loss of AvrSr50 by somatic exchange in stem rust leads to virulence for Sr50 resistance in wheat. Science **358**, 1607–1610.

Chen Y, Liu Z, Halterman DA. 2012. Molecular determinants of resistance activation and suppression by *Phytophthora infestans* effector IPI-O. PLoS Pathogens **8**, e1002595.

Collier SM, Hamel LP, Moffett P. 2011. Cell death mediated by the N-terminal domains of a unique and highly conserved class of NB-LRR protein. Molecular Plant-Microbe Interactions **24**, 918–931.

Conlan B, Stoll T, Gorman JJ, Saur I, Rathjen JP. 2018. Development of a rapid in planta BioID system as a probe for plasma membrane-associated immunity proteins. Frontiers in Plant Science **9**, 1882.

de la Concepcion JC, Franceschetti M, Maqbool A, Saitoh H, Terauchi R, Kamoun S, Banfield MJ. 2018. Polymorphic residues in rice NLRs expand binding and response to effectors of the blast pathogen. Nature Plants **4**, 576–585.

Dinesh-Kumar SP, Baker BJ. 2000. Structure–function analysis of the tobacco mosaic virus resistance gene N. Proceedings of the National Academy of Sciences, USA **97**, 14789–14794.

Dodds PN, Lawrence GJ, Catanzariti AM, Teh T, Wang CIA, Ayliffe MA, Kobe B, Ellis JG. 2006. Direct protein interaction underlies gene-for-gene specificity and coevolution of the flax resistance genes and flax rust avirulence genes. Proceedings of the National Academy of Sciences, USA **103**, 8888–8893.

Dodds PN, Rathjen JP. 2010. Plant immunity: towards an integrated view of plant–pathogen interactions. Nature Reviews. Genetics **11**, 539–548.

Förderer A, Li E, Lawson AW, *et al*. 2022a. A wheat resistosome defines common principles of immune receptor channels. Nature **610**, 532–539.

Förderer A, Yu D, Li E, Chai J. 2022b. Resistosomes at the interface of pathogens and plants. Current Opinion in Plant Biology **67**, 102212.

Gacek E. 1987. Distribution of barley powdery mildew resistance and virulence in Poland 1984–1986. Advances in Agricultural Biotechnology **2**, 93–98.

Gao Z, Chung EH, Eitas TK, Dangl JL. 2011. Plant intracellular innate immune receptor Resistance to *Pseudomonas syringae* pv.

maculicola 1 (RPM1) is activated at, and functions on, the plasma membrane. Proceedings of the National Academy of Sciences, USA **108**, 7619–7624.

Garcia AV, Blanvillain-Baufume S, Huibers RP, Wiermer M, Li GY, Gobbato E, Rietz S, Parker JE. 2010. Balanced nuclear and cytoplasmic activities of EDS1 are required for a complete plant innate immune response. PLoS Pathogens **6**, e1000970.

Gietz RD, Woods RA. 2002. Transformation of yeast by lithium acetate/single-stranded carrier DNA/polyethylene glycol method. Methods in Enzymology **350**, 87–96.

Glawe DA. 2008. The powdery mildews: a review of the world's most familiar (yet poorly known) plant pathogens. Annual Review of Phytopathology **46**, 27–51.

Grant M, Brown I, Adams S, Knight M, Ainslie A, Mansfield J. 2000. The RPM1 plant disease resistance gene facilitates a rapid and sustained increase in cytosolic calcium that is necessary for the oxidative burst and hypersensitive cell death. The Plant Journal **23**, 441–450.

Halterman DA, Wise RP. 2006. Upstream open reading frames of the barley Mla13 powdery mildew resistance gene function co-operatively to down-regulate translation. Molecular Plant Pathology **7**, 167–176.

Himmelbach A, Zierold U, Hensel G, Riechen J, Douchkov D, Schweizer P, Kumlehn J. 2007. A set of modular binary vectors for transformation of cereals. Plant Physiology **145**, 1192–1200.

Horsefield S, Burdett H, Zhang XX, *et al*. 2019. NAD^+ cleavage activity by animal and plant TIR domains in cell death pathways. Science **365**, 793–799.

Hovmøller MS, Caffier V, Jalli M, *et al*. 2000. The European barley powdery mildew virulence survey and disease nursery 1993–1999. Agronomie **20**, 729–743.

Huang S, Jia A, Song W, *et al*. 2022. Identification and receptor mechanism of TIR-catalyzed small molecules in plant immunity. Science **377**, eabq3297.

Jacob P, Kim NH, Wu F, *et al*. 2021. Plant 'helper' immune receptors are calcium ion-permeable nonselective cation channels. Science **373**, 420–425.

Jia A, Huang S, Song W, *et al*. 2022. TIR-catalyzed ADP-ribosylation reactions produce signaling molecules for plant immunity. Science **377**, eabq8180.

Jia Y, McAdams SA, Bryan GT, Hershey HP, Valent B. 2000. Direct interaction of resistance gene and avirulence gene products confers rice blast resistance. The EMBO Journal **19**, 4004–4014.

Jones JDG, Vance RE, Dangl JL. 2016. Intracellular innate immune surveillance devices in plants and animals. Science **354**, aaf6395.

Jorgensen JH. 1994. Genetics of powdery mildew resistance in barley. Critical Reviews in Plant Sciences **13**, 97–119.

Jørgensen JH, Hovmøller MS. 1987. Distribution of powdery mildew resistance and virulence in Denmark. Integrated control to reduce damage caused by cereal mildews. Advances in Agricultural Biotechnology **22**, 43–47.

Jubic LM, Saile S, Furzer OJ, el Kasmi F, Dangl JL. 2019. Help wanted: helper NLRs and plant immune responses. Current Opinion in Plant Biology **50**, 82–94.

Lapin D, Kovacova V, Sun X, *et al*. 2019. A coevolved EDS1–SAG101–NRG1 module mediates cell death signaling by TIR-domain immune receptors. The Plant Cell **31**, 2430–2455.

Lu XL, Kracher B, Saur IML, Bauer S, Ellwood SR, Wise R, Yaeno T, Maekawa T, Schulze-Lefert P. 2016. Allelic barley MLA immune receptors recognize sequence-unrelated avirulence effectors of the powdery mildew pathogen. Proceedings of the National Academy of Sciences, USA **113**, 6486–6495.

Ma S, Lapin D, Liu L, *et al*. 2020. Direct pathogen-induced assembly of an NLR immune receptor complex to form a holoenzyme. Science **370**, eabe3069.

Maekawa T, Cheng W, Spiridon LN, *et al*. 2011a. Coiled-coil domain-dependent homodimerization of intracellular barley immune receptors defines a minimal functional module for triggering cell death. Cell Host and Microbe **9**, 187–199.

Maekawa T, Kashkar H, Coll NS. 2022. Dying in self-defence: a comparative overview of immunogenic cell death signalling in animals and plants. Cell Death & Differentiation **30**, 258–268.

Maekawa T, Kracher B, Saur I, Yoshikawa-Maekawa M, Kellner R, Pankin A, von Korff M, Schulze-Lefert P. 2019. Subfamily-specific specialization of RGH1/MLA immune receptors in wild barley. Molecular Plant-Microbe Interactions **32**, 107–119.

Maekawa T, Kufer TA, Schulze-Lefert P. 2011b. NLR functions in plant and animal immune systems: so far and yet so close. Nature Immunology **12**, 817–826.

Mago R, Zhang P, Vautrin S, *et al*. 2015. The wheat Sr50 gene reveals rich diversity at a cereal disease resistance locus. Nature Plants **1**, 15186.

Märkle H, Saur IML, Stam R. 2022. Evolution of resistance (R) gene specificity. Essays in Biochemistry **66**, 551–560.

Martin R, Qi T, Zhang H, Liu F, King M, Toth C, Nogales E, Staskawicz BJ. 2020. Structure of the activated ROQ1 resistosome directly recognizing the pathogen effector XopQ. Science **370**, abd9993.

Moseman JG, Schaller CW. 1960. Genetics of the allelic aeries at the Mla locus in barley and cultures of *Erysiphe graminis* f. sp. *hordei* that differentiate these alleles. Phytopathology **50**, 736–741.

Nakagawa T, Kurose T, Hino T, Tanaka K, Kawamukai M, Niwa Y, Toyooka K, Matsuoka K, Jinbo T, Kimura T. 2007. Development of series of gateway binary vectors, pGWBs, for realizing efficient construction of fusion genes for plant transformation. Journal of Bioscience and Bioengineering **104**, 34–41.

Nishimura MT, Anderson RG, Cherkis KA, *et al*. 2017. TIR-only protein RBA1 recognizes a pathogen effector to regulate cell death in Arabidopsis. Proceedings of the National Academy of Sciences, USA **114**, E2053–E2062.

Ntoukakis V, Balmuth AL, Mucyn TS, Gutierrez JR, Jones AME, Rathjen JP. 2013. The tomato Prf complex is a molecular trap for bacterial effectors based on Pto transphosphorylation. PLoS Pathogens **9**, e1003123.

Ortiz D, Chen J, Outram MA, *et al*. 2022. The stem rust effector protein AvrSr50 escapes Sr50 recognition by a substitution in a single surface-exposed residue. New Phytologist **234**, 592–606.

Ortiz D, de Guillen K, Cesari S, Chalvon V, Gracy J, Padilla A, Kroj T. 2017. Recognition of the *Magnaporthe oryzae* effector AVR-Pia by the decoy domain of the rice NLR immune receptor RGA5. The Plant Cell **29**, 156–168.

Periyannan S, Moore J, Ayliffe M, *et al*. 2013. The gene Sr33, an ortholog of barley Mla genes, encodes resistance to wheat stem rust race Ug99. Science **341**, 786–788.

Plissonneau C, Daverdin G, Ollivier B, Blaise F, Degrave A, Fudal I, Rouxel T, Balesdent MH. 2016. A game of hide and seek between avirulence genes AvrLm4-7 and AvrLm3 in *Leptosphaeria maculans*. New Phytologist **209**, 1613–1624.

Rairdan GJ, Moffett P. 2006. Distinct domains in the ARC region of the potato resistance protein Rx mediate LRR binding and inhibition of activation. The Plant Cell **18**, 2082–2093.

Roberts M, Tang S, Stallmann A, Dangl JL, Bonardi V. 2013. Genetic requirements for signaling from an autoactive plant NB-LRR intracellular innate immune receptor. PLoS Genetics **9**, e1003465.

Rsaliyev A, Pahratdinova Z, Rsaliyev S. 2017. Characterizing the pathotype structure of barley powdery mildew and effectiveness of resistance genes to this pathogen in Kazakhstan. BMC Plant Biology **17**, 178.

Saile SC, Id PJ, Castel B, *et al*. 2020. Two unequally redundant 'helper' immune receptor families mediate *Arabidopsis thaliana* intracellular 'sensor' immune receptor functions. PLoS Biology **18**, e3000783.

Saur IM, Conlan BF, Rathjen JP. 2015. The N-terminal domain of the tomato immune protein Prf contains multiple homotypic and Pto kinase interaction sites. Journal of Biological Chemistry **290**:11258–11267. doi:10.1074/jbc.M114.616532.

Saur IML, Bauer S, Kracher B, *et al*. 2019a. Multiple pairs of allelic MLA immune receptor–powdery mildew AVRA effectors argue for a direct recognition mechanism. eLife **8**, e44471.

Saur IML, Bauer S, Lu X, Schulze-Lefert P. 2019b. A cell death assay in barley and wheat protoplasts for identification and validation of matching pathogen AVR effector and plant NLR immune receptors. Plant Methods **15**, 118.

Saur IML, Hückelhoven R. 2021. Recognition and defence of plant-infecting fungal pathogens. Journal of Plant Physiology **256**, 153324.

Saur IML, Panstruga R, Schulze-Lefert P. 2021. NOD-like receptor-mediated plant immunity: from structure to cell death. Nature Reviews. Immunology **21**, 305–318.

Seeholzer S, Tsuchimatsu T, Jordan T, Bieri S, Pajonk S, Yang WX, Jahoor A, Shimizu KK, Keller B, Schulze-Lefert P. 2010. Diversity at the Mla powdery mildew resistance locus from cultivated barley reveals sites of positive selection. Molecular Plant-Microbe Interactions **23**, 497–509.

Shao ZQ, Xue JY, Wu P, Zhang YM, Wu Y, Hang YY, Wang B, Chen JQ. 2016. Large-scale analyses of angiosperm nucleotide-binding site-leucine-rich repeat genes reveal three anciently diverged classes with distinct evolutionary patterns. Plant Physiology **170**, 2095–2109.

Shen QH, Saijo Y, Mauch S, Biskup C, Bieri S, Keller B, Seki H, Ulker B, Somssich IE, Schulze-Lefert P. 2007. Nuclear activity of MLA immune receptors links isolate-specific and basal disease-resistance responses. Science **315**, 1098–1103.

Shen QH, Zhou FS, Bieri S, Haizel T, Shirasu K, Schulze-Lefert P. 2003. Recognition specificity and RAR1/SGT1 dependence in barley Mla disease resistance genes to the powdery mildew fungus. The Plant Cell **15**, 732–744.

Shi W, Stolze SC, Nakagami H, Misas Villamil JC, Saur IML, Doehlemann G. 2023. Combination of *in vivo* proximity labeling and co-immunoprecipitation identifies the host target network of a tumor-inducing effector in the fungal maize pathogen *Ustilago maydis*. Journal of Experimental Botany **74**, doi:10.1093/jxb/erad188.

Slootweg EJ, Spiridon LN, Roosien J, *et al*. 2013. Structural determinants at the interface of the ARC2 and leucine-rich repeat domains control the activation of the plant immune receptors Rx1 and Gpa2. Plant Physiology **162**, 1510–1528.

Swiderski MR, Birker D, Jones JDG. 2009. The TIR domain of TIR-NB-LRR resistance proteins is a signaling domain involved in cell death induction. Molecular Plant-Microbe Interactions **22**, 157–165.

Tamborski J, Seong K, Liu F, Staskawicz B, Krasileva K. 2023. Altering specificity and auto-activity of plant immune receptors Sr33 and Sr50 via a rational engineering approach. Molecular Plant-Microbe Interactions **36**, doi:10.1094/MPMI-07-22-0154-R.

Wan L, Essuman K, Anderson RG, *et al*. 2019. TIR domains of plant immune receptors are NAD^+-cleaving enzymes that promote cell death. Science **365**, 799–803.

Wang JZ, Hu MJ, Wang J, Qi JF, Han ZF, Wang GX, Qi YJ, Wang HW, Zhou JM, Chai JJ. 2019a. Reconstitution and structure of a plant NLR resistosome conferring immunity. Science **364**, eaav5870.

Wang JZ, Wang J, Hu MJ, *et al*. 2019b. Ligand-triggered allosteric ADP release primes a plant NLR complex. Science **364**, eaav5868.

Williams SJ, Sohn KH, Wan L, *et al*. 2014. Structural basis for assembly and function of a heterodimeric plant immune receptor. Science **344**, 299–303.

Yu D, Song W, Tan EYJ, *et al*. 2022. TIR domains of plant immune receptors are 2′,3′-cAMP/cGMP synthetases mediating cell death. Cell **185**, 2370–2386.e18.

Zhang TT, Lei J, Yang HJ, Xu K, Wang R, Zhang ZY. 2011. An improved method for whole protein extraction from yeast *Saccharomyces cerevisiae*. Yeast **28**, 795–798.

Zhao YB, Liu MX, Chen TT, *et al*. 2022. Pathogen effector AvrSr35 triggers Sr35 resistosome assembly via a direct recognition mechanism. Science Advances **8**, 5108.